ANALYTICAL ASSESSMENT

FOR

EFFECTS OF LOOSE PARTS

ZION PLANT NO. 1

R. A. Hluhan

C. Yu

May 10, 1982

TABLE OF CONTENTS (Con't.)

TABLE OF CONTENTS (Con't.)

1.0 INTRODUCTION

The purpose of this study was to determine the potential effects on reactor internals and reactor pressure vessel of loose parts generated by the steam generator nozzle cover left in the hot leg inlet plenum of the ID steam generator at Commonwealth Edison's Zion Unit 1. These parts, assumed to have entered the reactor pressure vessel through an inlet nozzle, cause two specific concerns. The first is that a part may become wedged during cold shutdown and induce loads in core support structures during plant heatup. The second concern is that loads on reactor internals may be induced by impacting loose parts.

This report describes in detail the work performed to address the above concerns.

1.1 DESCRIPTION OF LOOSE PARTS

An inventory of missing loose parts believed to be in the reactor pressure vessel is given in Table 1.1-1.

TABLE 1.1-1 INVENTORY OF MISSING LOOSE PARTS

Part Description	Material	Number Missing
¼ - 20 x 3/4 long flat head bolt, nut and washer assembly (Figure 1-1)	Stainless Steel	21 assemblies plus one loose nut and one loose washer
3/4 x ½ x 0.06 Hinge Fragment (Figure 1-2)	Stainless Steel	1
1 1/16 x ½ x 0.06 Hinge Fragment (Figure 1-2)	Stainless Steel	1
¼ x 0.1 x 0.6 Hinge Fragment (Figure 1-2)	Stainless Steel	1
1/8 x ½ x 0.06 Hinge Fragment (Figure 1-2)	Stainless Steel	1
5/16 0 x ½ Long Hinge Fragment (Figure 1-2)	Stainless Steel	2

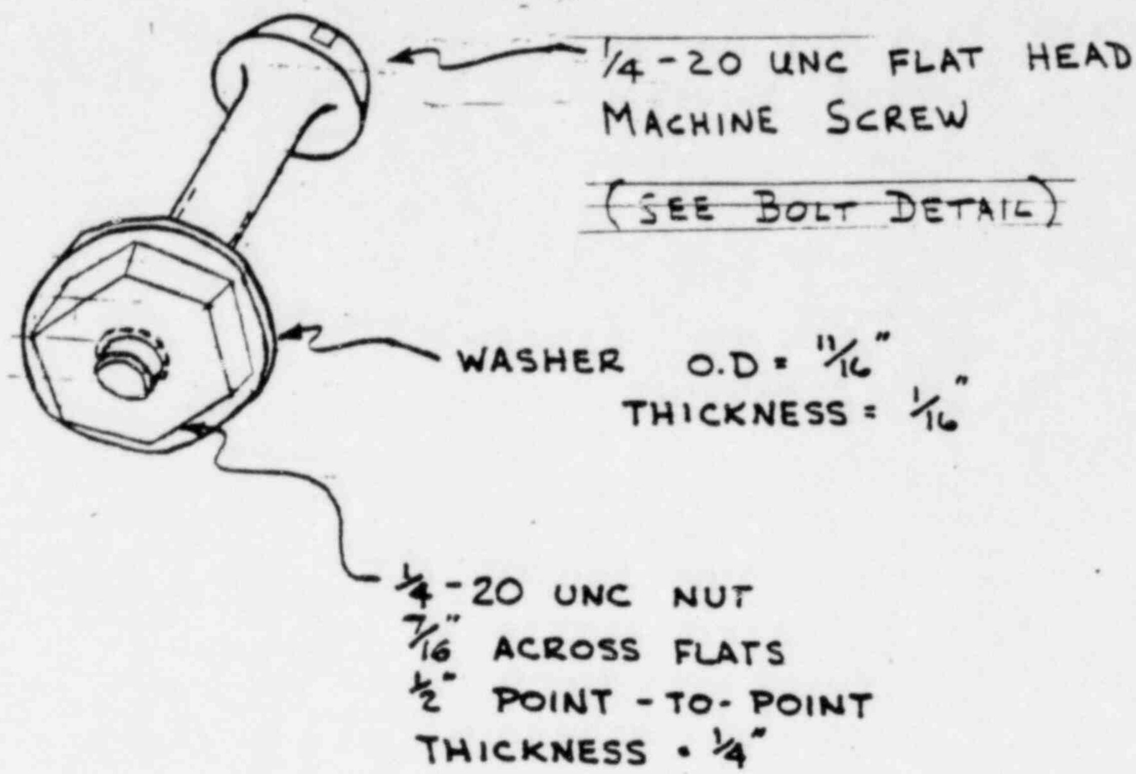

ALL PARTS STAINLESS STEEL
OVERALL LENGTH = 3/4 INCH
WEIGHT OF ASSEMBLY = 0.3 OUNCE

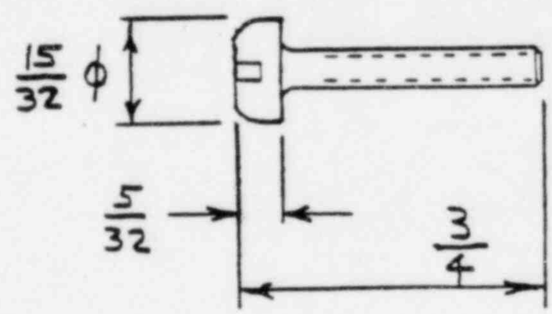

BOLT DETAIL

FIGURE 1-1 LOOSE BOLT ASSEMBLY

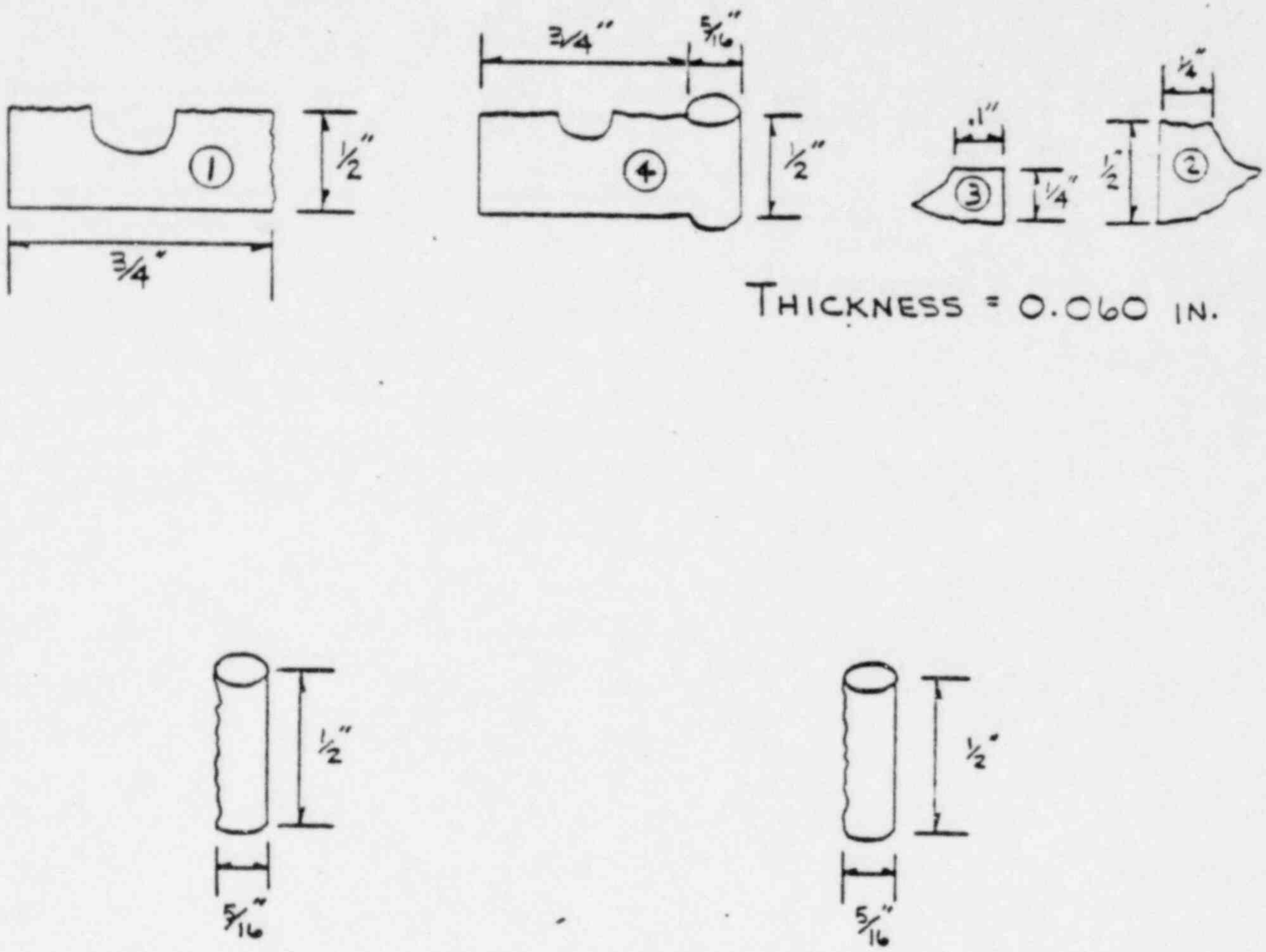

FIGURE 1-2 HINGE FRAGMENTS

It must be assumed that the bolt, nut and washer assemblies may be either together or separated, since parts were recovered in both conditions.

1.2 POTENTIAL LOOSE PARTS WEDGING LOCATIONS

A comprehensive study was made in order to determine possible loose part wedging locations along possible paths from an inlet nozzle to the lower core plate. Based on the size of the parts and reactor internals gap sizes, two significant wedging locations were discovered. The first location is the radial gap between the radial key and clevis insert. A radial key that is jammed due to loose parts may induce loads in the core barrel, radial keys and reactor pressure vessel during thermal transients. There is also a potential to violate the minimum core barrel flange to vessel ledge contact load thereby increasing the likelyhood of undesirable flow-induced vibrations.

The second wedging location identified was the gap between the secondary core support and inside vessel head. If relative motion of the reactor internals and vessel at this location becomes restricted due to interfering loose parts, loads are induced in these components. In addition there is again the possibility of violating the minimum core barrel flange to vessel ledge load thereby increasing the likelyhood of undesirable flow-induced vibrations.

1.3 POTENTIAL IMPACT TARGETS

Along with potential wedging locations for loose parts, possible impact locations were also identified. Three significant targets were identified as requiring detailed evaluation. These targets are

1) Core Barrel at Inlet Nozzle
2) Thermal Shield Flexure
3) Bottom Mounted Instrumentation Tube Penetrations

The three targets identified were evaluated for potential perforation and denting, as well as for overall structural response due to impact loads.

2.0 INTRODUCTION: POTENTIAL WEDGED PARTS EFFECTS

The following analysis was performed to assess the consequences of loose parts described in Section 1.1 being wedged at the two locations described in Section 1.2 and shown in Figure 2-1.

In the event that a part or parts becomes wedged during cold shutdown, loads are induced in the core support structures and reactor vessel during plant heatup. Six areas were identified as the most sensitive for loads caused by wedged parts between the radial key and clevis insert and between the secondary core support and inside vessel bottom head:

1) The secondary core support structure columns, or the energy absorbers; if yielding of an energy absorber occurs, the energy absorption capability may be reduced below the acceptable levels considered for postulated accidents.

2) The contact force between the core barrel flange and the reactor vessel ledge; a spring is provided at the core barrel flange and reactor vessel ledge to maintain a compressive force between the core barrel flange and the vessel ledge; if the compressive force is overcome or reduced substantially, (a minimum of 100,000 lbs. is desirable), an undesirable flow induced vibration condition could result.

3) The membrane, shear and bending stresses induced in the reactor vessel.

4) Yielding of radial keys; a single jammed key also induces stresses in the remaining free keys.

5) Core barrel stresses and critical buckling load.

6) The local stresses immediately under the wedged part and the effect on the vessel cladding.

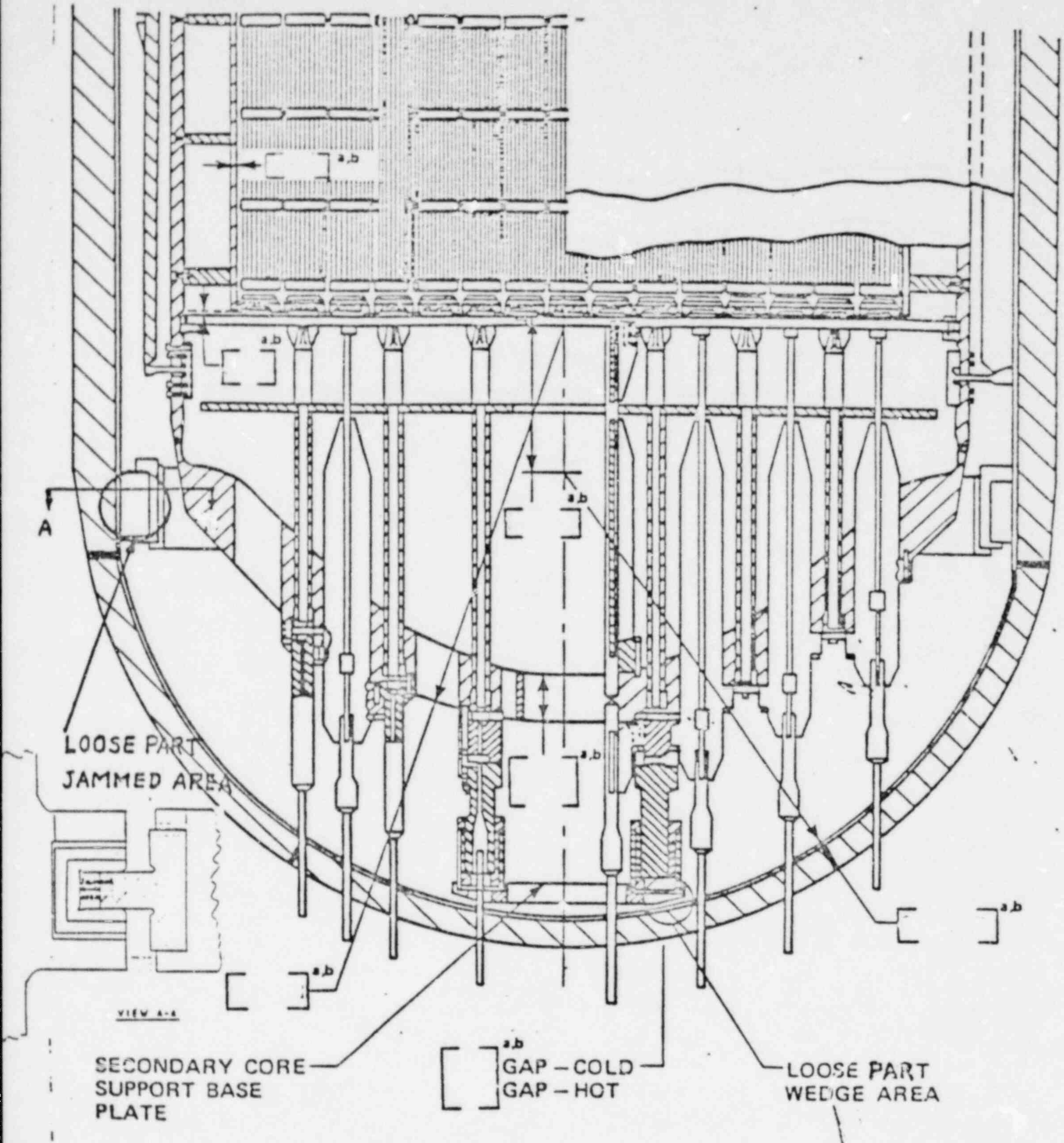

Figure 2-1. CWE Reactor Vessel, Lower Internals

An analytical evaluation program was performed to address the above areas and to determine heatup rates and pressures to preclude potential damage if parts become wedged. A five-step program was developed as outlined below:

1) Determine the load-deflection relationship for potential configurations of wedged loose parts. Since there are quite a number of possible configurations, testing was precluded due to a compressed time frame. Conservative load relationships for loose parts were determined by the analytical method outlined in Section 2.1.

2) A reactor vessel and internals vertical stiffness model was developed. The load deflection relationship for the specific wedged parts systems were used in the vertical stiffness model to estimate the loads induced by the wedged bolts. The allowable criteria used in the calculations for all cases is as follows:

   a. No yielding of the energy absorbers is permitted.

   b. The minimum net contact force between the core barrel flange and vessel ledge must be at least [ ][a,b] lbs. A reduced minimum value of the preload from the core barrel hold down spring which considers the measured permanent set in the spring of [ ][a,b] inch after the hot functional test was used to determine the existing contact force.

   The stiffness model is discussed in Section 2.2. The analysis to determine the contact force is discussed in Section 2.6.

3) A thermal analysis was performed to determine the minimum clearance between the reactor vessel and core support base plate during heat-up transients and a power increase to 100 percent power. The analysis and results are presented in Section 2.3.

4) An analysis was performed to determine the effect of the wedged parts on the stresses in the reactor vessel. The analysis is reported in Section 2.5.

5) Various pressure conditions and heatup rates between 0°F per hour and 100°F per hour were analyzed to determine the acceptable combinations of pressure and heatup rate. The analysis and results are presented in Sections 2.4 and 2.6, respectively.

6) The summary is presented in Section 2.7.

2.1 Determination of Wedged Loose Part Load-Deflection Relationships

The stiffness of the wedged loose part configuration is an important parameter in the analysis to determine loads induced in the internals and reactor vessel. The determination of this stiffness is a complex problem involving the prediction of both elastic and plastic behavior of the parts. The problem is further complicated by the fact that there are numerous parts and they may tend to congregate and fill gaps by stacking up. Therefore, the following conservative assumption is made in order to simplify this task.

Assumption (1):

Since the parts are small and cannot sustain high loads elastically, they will deform plastically. Since crush tests are not performed it must be conservatively assumed that the wedged parts sustain their ultimate load carrying capability for the wedging conditions considered. An ultimate strength of 63.5 ksi is used for all temperatures.

2.1.1 Load-Deflection Relationship for Wedged Bolt Head

The load deflection curve for the bolt head is determined by calculating its ultimate load capacity for given degrees of deformation. The bolt head is conservatively idealized as a cylinder with the dimensions shown in Figure 2.1-1.

Conservatively assuming that the vessel and internals contact surfaces are rigid, the load deflection curve for the bolt head is developed in the following manner.

Assuming that both contact surfaces of the bolt head deform equally, the contact area of the bolt head is calculated for varying degrees of deformation (δ) as shown in Figure 2.1-2.

$$r_B - \delta = \tfrac{1}{2}[4r_B^2 - w^2]^{\frac{1}{2}} \qquad \text{(Eq. 2.1)}$$

$$\delta = r_B - \tfrac{1}{2}[4r_B^2 - w^2]^{\frac{1}{2}} \qquad \text{(Eq. 2.2)}$$

Solving for w:

$$w = [4\,\delta(2r_B - \delta)]^{\frac{1}{2}} \qquad \text{(Eq. 2.3)}$$

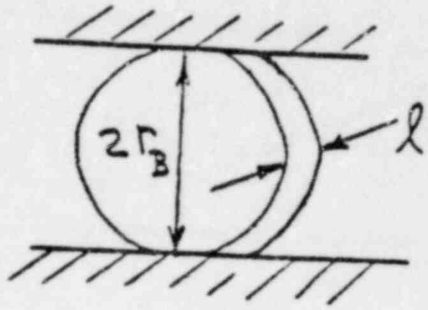

r_B = 15/64 inch

ℓ = ½ inch

FIGURE 2.1-1 IDEALIZED WEDGED BOLT HEAD

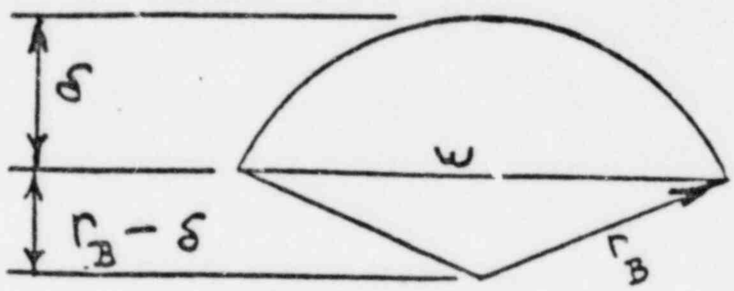

FIGURE 2.1-2 BOLT HEAD WIDTH AND DEFLECTION

Since both contact surfaces of the bolt deform equally, the total compression of the bolt, δ_B, is equal to 2δ. The load corresponding to this bolt compression is calculated by multiplying the bolt contact area by the ultimate strength of the bolt material. Therefore, the load-deflection relationship for the bolt head compression is given by Equation 2.4.

$$\frac{P}{\ell\sigma_{ULT}} = [\frac{4\delta_B}{2}(2r_B - \frac{\delta_B}{2})]^{\frac{1}{2}}$$

or

$$P = \ell\sigma_{ULT}[2\delta_B(2r_B - \frac{\delta_B}{2})]^{\frac{1}{2}} \qquad \text{(Eq. 2.4)}$$

2.1.2 <u>Load-Deflection Relationship for Wedged Nuts, Washers and Hinge Fragments</u>

Since an area-deformation relationship determination for these parts is at best extremely complicated, it is assumed that these parts deform plasticly at constant area (constant load). Again assuming rigid vessel and internals contact surfaces the maximum load due to wedged nuts, washers and hinge fragments is determined for each piece by multiplying its effective area by the ultimate strength of 63.5 ksi. The areas and maximum loads determined for these parts are listed in Table 2.1-1 and the geometries of the wedged parts are shown in Figures 2.1-3 through 2.1-7.

TABLE 2.1-1

PART	SUB-CONFIGURATION	EFFECTIVE AREA (IN^2)	MAX. LOAD (LB)
Nut	I (Figure 2.1-5)	0.132	8382
Nut	K (Figure 2.1-5)	0.1095	6953
Washer	J (Figure 2.1-5)	0.3220	20447
Hinge Fragments	B (Figure 2.1-3)	0.3308	21006

SUB - CONFIGURATION A ONE BOLT HEAD AND ONE WASHER

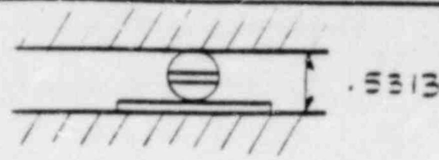

$F_{MAX} = 7430$ Lb (HOT)

SUB - CONFIGURATION B HINGE FRAGMENTS

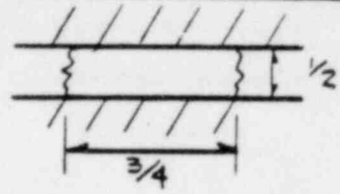

(2) PARTS

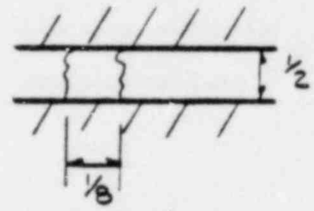

(1) PART

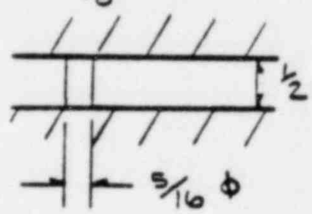

(3) PARTS

$$\text{CONTACT AREA} = \left\{ 2\left[.75(.062)\right] + \left[.125(.062)\right] + 3\left[\frac{\pi}{4}\left(\frac{5}{16}\right)^2\right] \right\}$$

$$= .3308 \text{ IN}^2$$

$$F_{MAX} = .3308\,(63500)\text{ Lb} = 21006 \text{ Lb}$$

SUB - CONFIGURATION C TWO NUTS

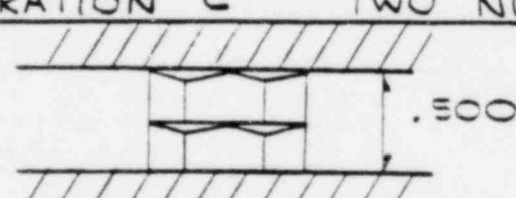

$F_{MAX} = 8382$ Lb (HOT)

SUB-CONFIGURATION D ONE BOLT

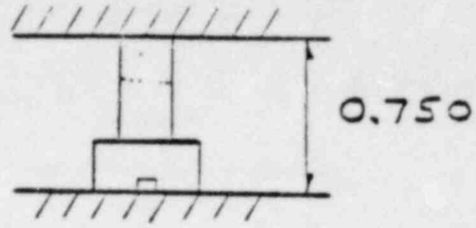

FMAX = 1778 Lb

SUB-CONFIGURATION E EIGHT WASHERS

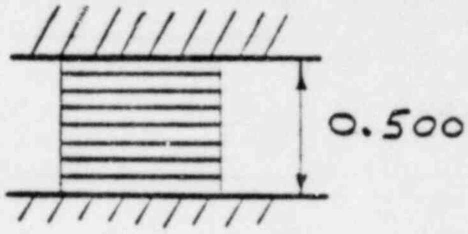

FMAX = 20447 Lb

SUB-CONFIGURATION F SEVEN WASHERS AND TWO HINGE FRAGME

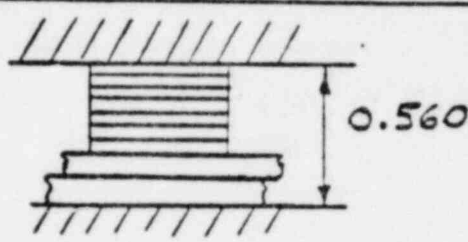

FMAX = 18733 Lb

SUB-CONFIGURATION G THREE NUTS

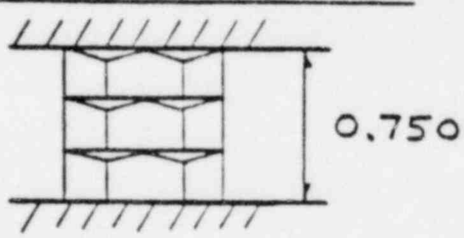

FMAX = 8382 Lb

SUB-CONFIGURATION H TWO NUTS AND ONE HINGE FRAGMENT

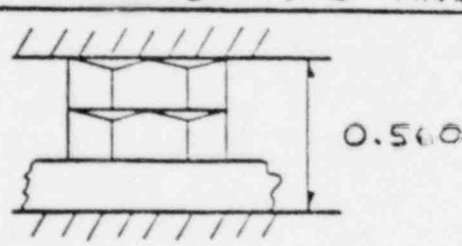

FMAX = 8382 Lb

SUB-CONFIGURATION I (SINGLE NUT)

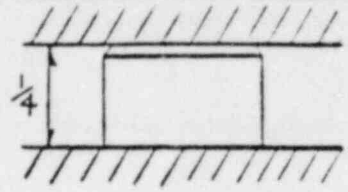

CONTACT AREA : $\left\{ \tfrac{7}{16}(.242) - (\tfrac{7}{32})\tfrac{1}{2}(.50-.242)2 - \tfrac{\pi}{4}(.196)^2 \right\}$ IN^2

$= .132$ IN^2

$F_{MAX} = .132(63500)$ Lb $=$ **8382 Lb**

SUB-CONFIGURATION J SINGLE WASHER

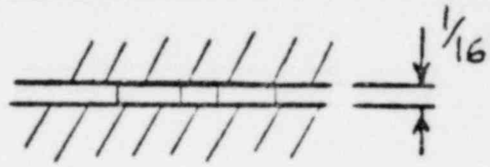

CONTACT AREA $= \tfrac{\pi}{4}\left\{(\tfrac{11}{16})^2 - (.25)^2\right\}$ IN^2 $= .3220$ IN^2

$F_{MAX} = 20447$ Lb

SUB-CONFIGURATION K SINGLE NUT

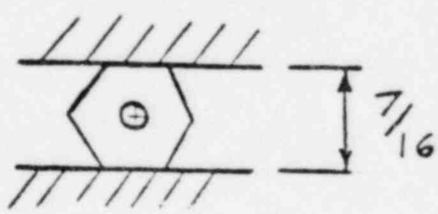

CONTACT AREA $= 0.438(0.25)$ IN^2 $= 0.1095$ IN^2

$F_{max} = 6953$ Lb

FIGURE 2.1-6 LOOSE PARTS SUB-CONFIGURATION L

SUB-CONFIGURATION L (VERTICAL STACKING)

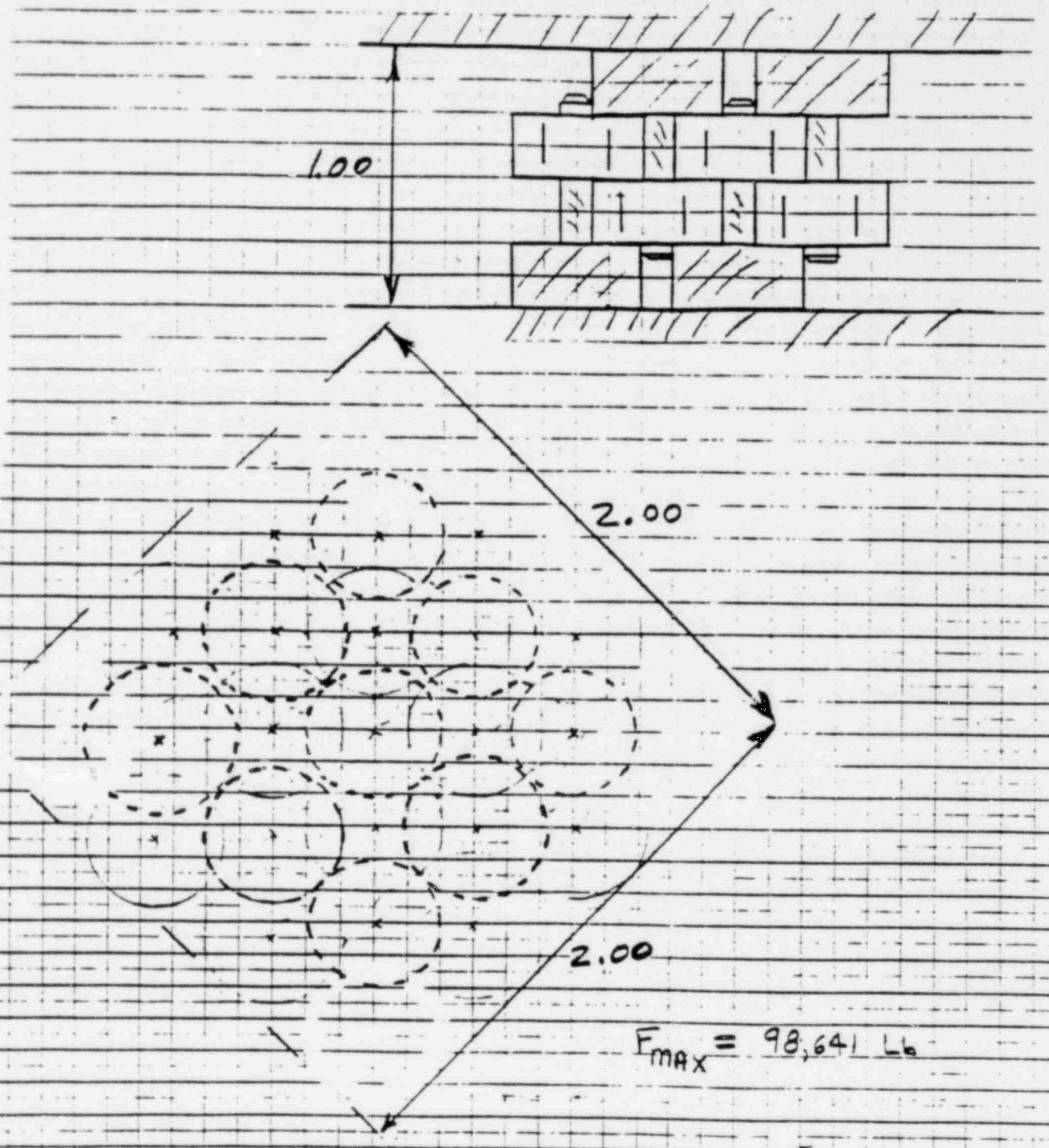

TOP VIEW OF STACKING ARRANGEMENT (21 ASSEMBLIES)

FIGURE 2.1-7 LOOSE PARTS SUB-CONFIGURATIONS M-O

SUB-CONFIGURATION M

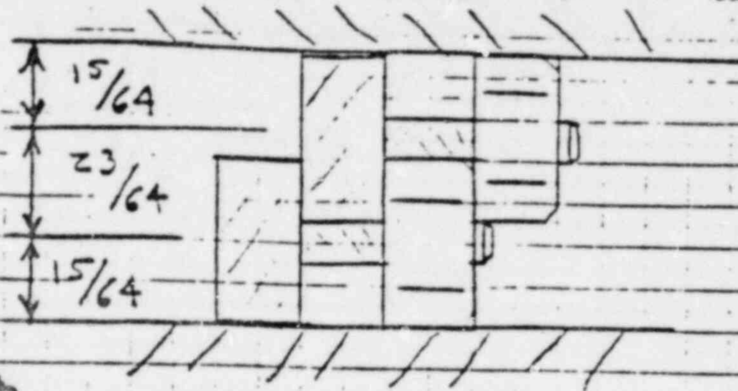

HEIGHT = 0.828

F_{MAX} = 9335 Lb

SUB-CONFIGURATION N SINGLE WASHER

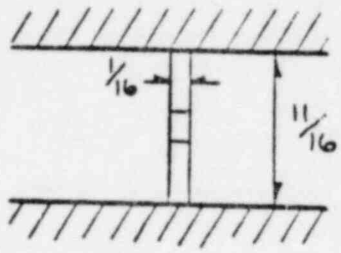

CONTACT AREA = $(\frac{11}{16} - \frac{1}{4})(\frac{1}{16})$ IN^2 = 0.0273 IN^2

F_{MAX} = .0273 (63,500) Lb. = 1734 Lb (HOT)

SUB-CONFIGURATION O SINGLE BOLT HEAD

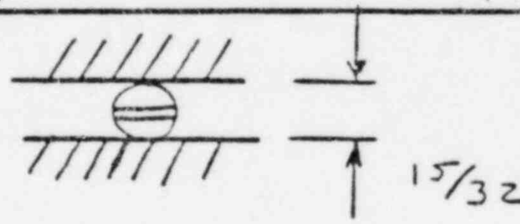

2.2 REACTOR VESSEL AND INTERNALS STIFFNESS MODEL

2.2.1 Introduction

The vertical stiffness model for the vessel/internals is implemented to determine forces and deformations resulting from bolts wedged between the secondary core support plate and vessel bottom head. The spring model includes the cross-sectional stiffnesses of the various sections of the reactor vessel and lower internals. Table 2.2-1 tabulates the spring constant values of each component included in the mathematical model. The calculated spring quantities are known from previous work performed for Consolidated Edison in support of the loose part in the IPP-II reactor vessel in March 1978.[1]

2.2.2 Stiffness Analysis

The assumption used to determine the stiffness of each sub-component of the reactor vessel and internals is described in Reference 30. The numerical values of the various springs are tabulated in Table 2.2-1. The values in Table 2.2-1 are for 70°F and must be corrected for the actual average temperature associated with each transient or steady state condition analyzed. The correction factor to be multiplied by each spring is the ratio of the modulus of elasticity at the average component temperature (through the component thickness) to the modulus of elasticity at 70°F. Section 2.3 provides the average temperature distribution for the vessel and internals for various transient and steady-state temperature conditions. Thus, in the analysis, the spring constants are variables that depend on the temperature condition being analyzed.

Table 2.2-1

VERTICAL SPRING CONSTANTS

Element	Description	K
Vessel		a,b
k_n	Nozzle shell course	
k_s	Vessel shell course	
k_h	Vessel head	
Internals		
k_{cbf}	Core barrel flange	
k_{cbw}	Core barrel shell	
k_{lsp1}	Lower support plate (one absorber acting)	
k_{lsp4}	Lower support plate (four absorbers acting)	
k_{eac}	Energy absorber cylinder, Housing, and Guide Post	
k_{ear}	Energy absorber Ligament	
k_{eap}	Base Plate	
Bolt Systems		
K_{SB}	Bolt and local stiffness of base plate, vessel, and vessel clad as a system	

Refer to Figures 2.2-2 and 2.2-3 for correlation to actual parts.

0583E:1

Figure 2.2-1 and 2 show the spring system of the reactor vessel and internals, and the load paths associated with a wedged bolt. As shown, a compression load path exists in the reactor internals, and a tension load path exists in the reactor vessel (the stiffness calculations include shear and bending distortions as appropriate in the vessel head, and other components in the load paths).

As shown on figure 2.2-1 the tension load path is comprised of the vessel barrel and the lower spherical head. The vessel load path is comprised of three springs.

System Stiffness of Vessel

$$K_{sv\,(cold)} = 1/\left(\frac{1}{k_n} + \frac{1}{k_s} + \frac{1}{k_h}\right) = [\qquad]^{a,b}$$

Corrected for lower modulus at 550°F,

$$K_{sv\,(hot)} = [\qquad]^{a,b}$$

The upper internals load path can be viewed as consisting of two regions: the upper internals structure load path, or the portion above the core support casting; and the lower support load path region, or the portion below the core support casting. Each region is discussed separately.

System Stiffness Above Lower Core Support Casting.

The upper load path region consists of two parallel load paths as shown on figure 2.2-1. The load path indicated by a dashed line, composed of the fuel assemblies, and upper internals structure, has been shown by previous analysis to have a spring rate much less than the load path indicated by a solid line on figure 2.2-1, and has been neglected in the analysis. The spring rate for the upper barrel region is then comprised of the load path shown by a solid line in figure 2.2-1, and is given by:

$$K_1 = 1/\left(\frac{1}{k_{cbw}} + \frac{1}{k_{cbf}}\right)$$

System Stiffness Below the Core Barrel

The spring system below the casting consists of three elements: the core support casting; the energy absorber cylinders and the energy absorbers. The spring rate varies and is dependent on the number of absorbers that are acting.

For four (4) absorbers the value is:

$$K_2 = 1/\left(\frac{1}{k_{lsp4}} + \frac{1}{(4)k_{eac}} + \frac{1}{(4)k_{ear}}\right), \text{ and}$$

For one (1) energy absorber the value is:

$$K_2 = 1/\left(\frac{1}{k_3} + \frac{1}{k_{lspl}}\right)$$

where:

$$k_3 = k_4 + k_5$$

$$k_4 = 1/\left(\frac{1}{k_{eac}} + \frac{1}{k_{ear}}\right)$$

$$k_5 = 1/\left(\frac{1}{2k_4} + \frac{1}{k_{eap}}\right)$$

Refer to Figure 2.2-3.

The overall system stiffness of lower internals is;

$$K_{SI} = \frac{1}{1/K_1 + 1/K_2}$$

For four (4) absorbers acting the overall system stiffness is:

K_{SI} = [ ]^{a,b} and,
(cold)

K_{SI} = [ ]^{a,b}
(hot)

For one (1) absorber acting, the overall system stiffness of lower internals is:

$$K_{SI} = \left[\qquad\qquad\qquad\qquad \right]^{a,b} \text{and,}$$

(cold)

$$K_{SI} = \left[\qquad\qquad\qquad\qquad \right]^{a,b}$$

(hot)

Figure 2.2-3 shows the idealized final spring model for the system. In the model, K_{SB} is the stiffness for the wedged part system: and

$$K_{SBV} = \frac{1}{1/K_{SB} + 1/K_{SV}}$$

The value δ_p is the potential interference with the part. δ_p is the part height, minus the gap between the reactor vessel and the lower support base plate calculated for each temperature and pressure condition evaluated. Section 2.4 discusses the calculation for δ_p.

Using the fact that the force (F) acting on the springs, K_{SI} and K_{SBV}, must be equal and opposite forces, and that

$\delta_p = \Delta_1 + \Delta_2$, then;

$$\delta_p = \frac{F}{K_{SI}} + \frac{F}{K_{SBV}} \quad , \text{ or}$$

$$F = \delta_p / \left(\frac{1}{K_{SI}} + \frac{1}{K_{SBV}}\right)$$

Substituting the previously stated relationship for K_{SBV} in terms of K_{SB} and K_{SV} results in

$$F = \delta_p / \left(\frac{1}{K_{SI}} + \frac{1}{K_{SV}} + \frac{1}{K_{SB}}\right)$$

Thus, the force (F) acting on the internals and the vessel can be simply evaluated for a specific value of δ_p, the potential interference, and for a specified value K_{SB}, the stiffness of the wedged part system. The load deflection curve, as discussed in Section 2.1 is non-linear, and the appropriate value of K_{SB} is initially unknown. An iterative procedure is employed to determine the appropriate value of K_{SB} and the resulting force induced in the system for a specified δ_p.

2.2.3 Summary

A comprehensive spring model was developed that considers the stiffness of the individual structural elements in the load path for the internals and vessel for forces induced by a wedged bolt. The stiffness of the vessel structure elements and internals structural elements are corrected for the average temperature for each thermal condition analyzed.

An iterative procedure is employed to account for the non-linear load-deflection curve of the wedged part system. The force induced in the reactor vessel and the internals is determined for the potential interference that exists with the parts for any specific thermal and pressure condition. The calculation of the potential interference that exists with the parts for any specific thermal and pressure condition (part height minus the gap between the vessel and the lower core support base plate) is discussed in Section 2.4. The forces calculated for various temperature and pressure conditions are discussed in Section 2.6.

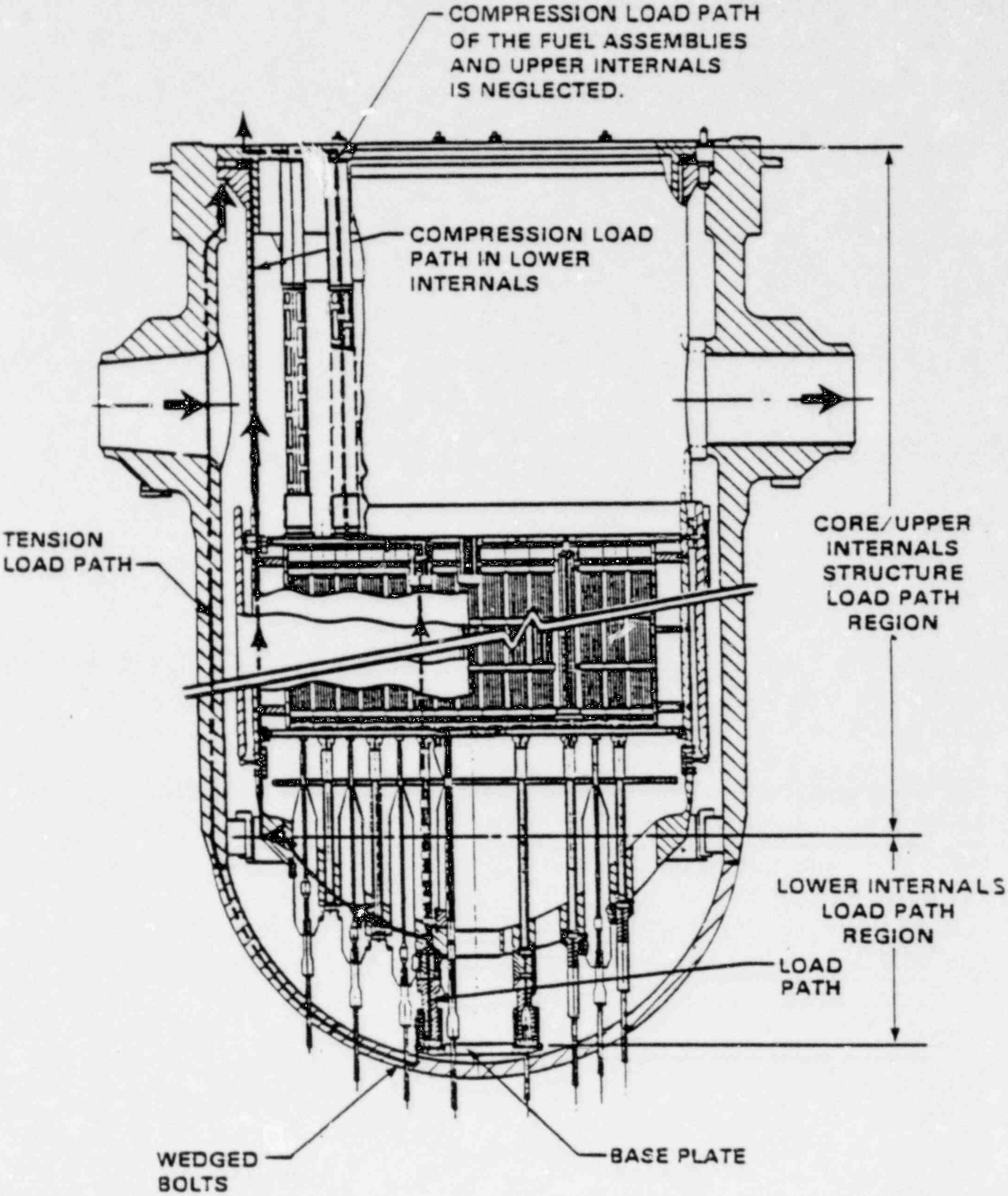

FIGURE 2.2-1 LOAD PATH IN LOWER INTERNALS FROM WEDGED BOLTS

19,178-39

a,b

1) DIMENSIONS ARE USED IN CALCULATING AXIAL ΔL OF VESSEL DUE TO OPERATING PRESSURE-IN INCHES.

2) DIMENSIONS ARE USED IN CALCULATIONS FOR AXIAL THERMAL EXPANSION-IN INCHES.

Figure 2.2-2 Core Barrel Assembly – Vessel Mathematical Model (Four Energy Absorbers Under Load)

a,b

1) DIMENSIONS ARE USED IN CALCULATING AXIAL ΔL OF VESSEL DUE TO OPERATING PRESSURE-IN INCHES.

2) DIMENSIONS ARE USED IN CALCULATIONS FOR AXIAL THERMAL EXPANSION-IN INCHES.

Figure 2.2-3 Core Barrel Assembly – Vessel Mathematical Model (One Energy Absorber Under Load)

[ ] a,b

Figure 2.2-4 Vertical Stiffness Model of Internals, Wedged Part, Vessel System

2.3 THERMAL ANALYSIS FOR TRANSIENT TEMPERATURE CONDITIONS

An important parameter in the analysis is the relative growth that takes place between the reactor internals, (core barrel, support structure, etc) and the reactor vessel during temperature changes. As shown on figure 2-1, the significant relative growth is that which takes place between the core barrel support ledge and the bottom of the vessel.

As shown on Figure 2.2-2, the core barrel is essentially a cylinder with an approximate thickness of 2.25 inches for its significant length and the reactor vessel is composed of three areas:

1) the bottom head which is 5.5 inches thick;

2) the cylinder below the inlet and outlet nozzles which is 9 inches thick; and

3) the cylinder above the nozzles which is 11.0 inches thick.

In addition, the core barrel is 304 stainless steel, while the reactor vessel is carbon steel. Because of the differences in the thicknesses and the difference in material, the average temperature in the reactor vessel will always be lower than the core barrel during transient heat-up conditions. Thus, the gap between the lower core support structure and the bottom reactor vessel head will be smaller during transient heat-up conditions, than during steady state conditions.

A thermal analysis was performed to estimate the average temperature difference between the core barrel and the reactor vessel to conservatively predict the minimum gap between the core support and vessel during the heat-up transients.

2.3.1 ANALYSIS MODELS - THERMAL

Figure 2.2-2 shows the actual core barrel and reactor vessel configuration The core barrel is essentially a cylinder of constant thickness equal to 2.25 inches from the core barrel support ledge to the top of the core barrel support keys. Below the support keys, the core support structure and core barrel is composed of materials of various thicknesses, which are greater than 2.25 inches. Therefore, assuming that these lower structures are all 2.25 inch thick will over predict the internals average temperature, which in turn will conservatively over predict the closure of the gap between the vessel and internals structure during the transient. The models considered in the thermal analysis are shown in Table 2.3-1. As indicated in Table 2.3-1, an analysis was performed for each of the reactor vessel thicknesses.

Table 2.3-1

THERMAL MODELS

COMPONENT	INNER RADIUS (INCHES)	WALL THICKNESS (INCHES)
Reactor Vessel (Carbon Steel)	86.5	5.5, 9.0, 11.0
Core Barrel (Stainless Steel)	74.5	2.25

One-dimensional thermal models, using the WECAN[4] computer program were used to obtain the reactor vessel and core barrel radial temperature distribution during the transient heat-up conditions. Each model consists of 10 elements through the wall thickness to estimate the radial temperature distribution. A post processor, a modified version of ATEMP35, was used to convert the radial temperature distribution into an average temperature. ATEMP35 computes a weighted average, where the weighting function accounts for the increase in area associated with the increased radius of each of the 10 elements through the vessel thickness.

The one-dimensional thermal models correspond to assuming that the reactor coolant temperature is constant along the axis of the reactor vessel.

The heatup is from an initial temperature of 70°F to a final temperature of 550°F. Heatup rates ranging from 20°F/hr to 100°F/hr were considered. A heat transfer coefficient, (h), of 3000 BTU/hr-ft^2-°F was applied to the ID of the reactor vessel and the OD of the core barrel. At the ID surface of the core barrel, a "h" of 500 BTU/hr-ft^2-°F was applied. The lower "h" for the ID of the core barrel is a result of the lower coolant flow rate at the inside surface. The OD surface of the reactor vessel was assumed to be adiabatic. As subsequently discussed in Section 2.3.2, the data obtained for the heat-up from 70°F to 550°F can be used directly to obtain the temperature differences for a heat-up of 70°F to 350°F and 70°F to 450°F.

2.3.2 TEMPERATURE DISTRIBUTION FOR HEAT-UP TRANSIENTS

The maximum temperature difference between the reactor vessel and the core barrel occurs at the end of the heat-up ramp when the coolant fluid temperature just reaches the 550°F temperature. Figures 2.3-1 through 2.3-5 show the temperature time histories for the three reactor vessel thicknesses and the core barrel, for heatup rates of 20°F/hr, 30°F/hr, 50°F/hr, 80°F/hr and 100°F/hr, respectively. The maximum temperature lag for heat-up to 550°F for the various thicknesses as a function of heat-up rate are shown on Figure 2.3-6. As seen on Figure 2.3-6, the temperature lag as a function of heat-up rate can be approximated as a straight line that intersects the temperature axis at 550°F for each thickness. Therefore, the temperature lag for each thickness, for any heat-up rate can be read directly from Figure 2.3-6.

As previously discussed, the maximum temperature lag for each thickness occurs at the end of the heat-up transient, when the fluid temperature just reaches its steady state condition. The calculations were performed for a steady state temperature of 550°F; however, the temperature lags for lower steady state conditions can be read directly from Figures 2.3-1 through 2.3-5. The appropriate temperature for each of the thicknesses is the temperature at the time when the fluid just reaches the desired steady state temperature less than 550°F. See Figures 2.3-1 through 2.3-5.

Two other intermediate steady state conditions were also evaluated. They are: 70°F to 350°F and 70°F to 450°F. For both of these conditions, the temperature lag for each thickness versus rate of heat-up were developed. The curves for the two conditions are shown on Figure 2.3-7 for the 70°F to 450°F condition, and on Figure 2.3-8 for the 70°F to 350°F condition.

The average temperature for each thickness of the reactor vessel, and for the core barrel (internals) from Figures 2.3-6, 2.3-7 and 2.3-8 are used in the subsequent analysis to determine the relative thermal growth of the reactor vessel and core barrel (internals) for the various heat-up rates considered in this study.

2.3.3 STEADY STATE TEMPERATURE DISTRIBUTION FOR VARIOUS LEVELS OF POWER

During increases in power levels, the outlet temperature (hot leg) and the inlet temperature (cold leg) are assumed to have a linear variation with the power level as shown on Figure 2.3-9. The hot leg temperature (T_{HL}) and the cold leg temperature (T_{CL}) at any power level can be calculated from

$$T_{HL} = T_H + \frac{P}{100}(T_{HL,100} - T_H); \text{ and,}$$

$$T_{CL} = T_H + \frac{P}{100}(T_{CL,100} - T_H); \text{ and,}$$

$$T_{AVG} = \frac{T_{HL} + T_{CL}}{2}$$

The reactor vessel and internals are separated into three regions for the purpose of evaluating the average temperature in the internals. The three regions, as shown on Figure 2.3-10 are:

1) upper barrel region;
2) middle barrel region; and
3) the lower core support assembly region.

The entire reactor vessel and the lower core support assembly will tend to follow the cold leg temperature during power increases.

Thus, the average temperature for the reactor vessel and lower support assembly is

$$T_1 = T_{CL}$$

The upper core barrel is exposed to both the hot leg and cold leg fluid. Therefore the upper barrel temperature (T_2) will tend to be the average temperature of the hot leg and cold leg, or

$$T_2 = T_{AVG}$$

The middle core barrel is also exposed to both the hot leg and cold leg temperatures. However, in the middle barrel region, there is a significant amount of gamma heating which raises the average middle barrel temperature by 35 degrees above the inlet temperature at one hundred percent power. The middle barrel temperature at any power level is determined by proportioning the 35 degree increase at 100 percent power and the level of power (i.e. the average tsmperatures of the middle barrel at 10 percent power is 3.5 degrees above the inlet temperature).

The size of the gap between the secondary core support and thes inside vessel head is plotted as a function of power level at various pressures in Figure 2.4-2.

a,b

AVERAGE TEMPERATURE (°F)

TIME (HOURS)

Figure 2.3-1 Thermal Response to 100 Degree Per Hour Heatup Transient

a,b

AVERAGE TEMPERATURE (°F)

TIME (HOURS)

Figure 2.3-2 Thermal Response to 80 Degree Per Hour Heatup Transient

TEMPERATURE (°F)

TIME (HOURS)

Figure 2.3-3 Thermal Response to 50 Degree Per Hour Heatup Transient

a,b

AVERAGE TEMPERATURE (°F)

TIME (HOURS)

Figure 2.3-4 Thermal Response to 30 Degree Per Hour Heatup Transient

a,b

AVERAGE TEMPERATURE (°F)

TIME (HOURS)

Figure 2.3-5 Thermal Response to 20 Degree Per Hour Heatup Transient

a,b

AVERAGE TEMPERATURE (°F)

HEATUP RATE (°F/HOUR)

Figure 2.3-6 4L Heatup Transient Temperatures at End of Heatup Ramp When CB/RV ΔT_{MAX} Occurs (70°F to 550°F)

[ ]a,b

AVERAGE TEMPERATURE (°F)

HEATUP RATE (°F/HOUR)

Figure 2.3-7 4L Heatup Transient Temperature at End of Heatup Ramp When CB/RV ΔT_{MAX} Occurs (70°F to 450°F)

a,b

AVERAGE TEMPERATURE (°F)

HEATUP RATE (°F/HOUR)

Figure 2.3-8 4L Heatup Transient Temperatures at End of Heatup Ramp When CB/RV ΔT_{MAX} Occurs (70°F to 350°F)

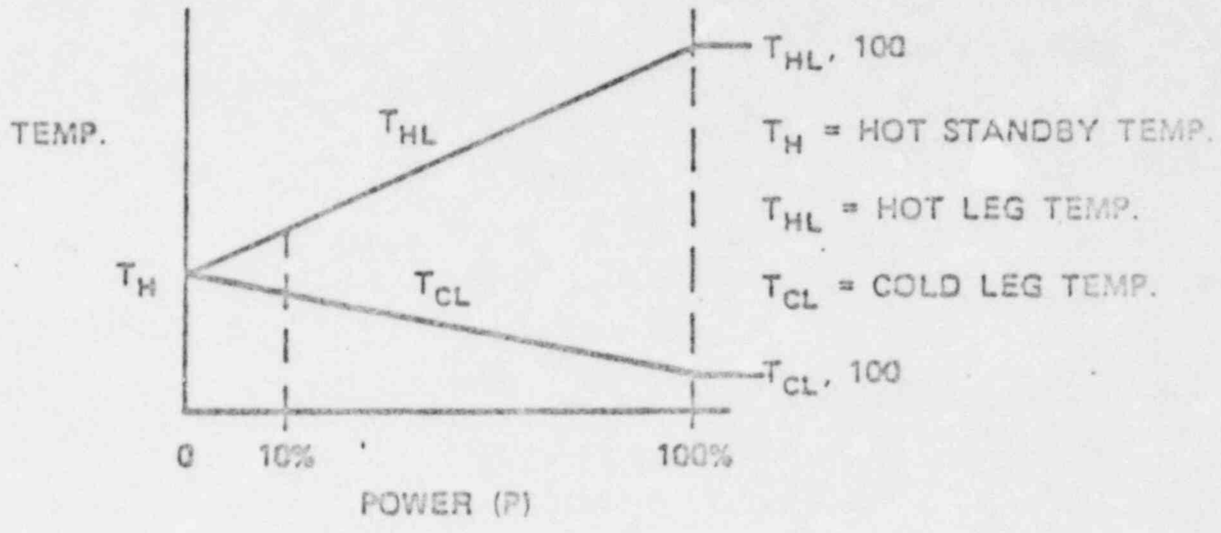

Figure 2.3-9 Temperature versus Power Relationship

a,b

Figure 2.3-10 Temperature Zones in Lower Internals and Vessel are Given for 10% Power

2.4 Analysis to Predict Gap for Various Temperature - Pressure Conditions

The gap between the secondary core support base plate and vessel bottom head is in part based on relative growth that has taken place between the lower internals and reactor vessel during heat-up changes. As shown on Figure 2.2-1 and 2, only the growth which takes place between the core barrel vessel support ledge and the bottom of the vessel head is significant.

The magnitude of the gap is also a result of the operating pressure applied to the vessel wall and bottom vessel head.

The potential interference needed for the analysis discussed in Section 2.2, is the difference between the part height and the gap determined for each temperature and pressure condition. After the gap and the potential interference are determined the force applied at the vessel ledge, energy abosrbers, and bottom vessel head are calculated using the stiffnesses determined in Sections 2.1 and 2.2.

The as-built readings recorded prior to hot functional test between the secondary core support base plate and reactor vessel gave a minimum gap of 1.030 inches. These readings were taken prior to the addition of the fuel. An analysis was performed to determine the reduction in the gap (additional extension of the core barrel assembly from the vessel ledge) due to the added buoyant weight of the fuel. The analysis consists of loading the spring model shown on Figure 2.2-1 and 2 with the appropriate fuel weight. The calculated reduced cold gap is [ ]^{a,b} inches.

2.4.1 RELATIVE THERMAL EXPANSION

The differential thermal growth for the vessel and lower internals from the core barrel flange vessel ledge defines the reduced thermal gap as follows:

$\Delta L = \Delta L_1 - \Delta L_2 - \Delta L_3 - \Delta L_4$ = Reduction in gap due to thermal condition

$$\Delta L_1 = \alpha_1 L_1 (T_1 - 70)$$
$$\Delta L_2 = \alpha_2 L_2 (T_2 - 70)$$
$$\Delta L_3 = \alpha_3 L_3 (T_3 - 70)$$
$$\Delta L_4 = \alpha_4 L_4 (T_4 - 70)$$

where

ΔL_1 = length of lower internals measured from the vessel ledge to the bottom of the lower support structure (see figure 2.2-2)

T_1 = Indicated average temperatures of the internals structure obtained from section 2.3.2 during heat-up transient conditions.

$\Delta L_2 \Delta L_3 \Delta L_4$ = Refer to figure 2.2-2 for the appropriate lengths.

T_i = Indicated temperatures of the vessel obtained from section 2.3.2 during heat-up transient conditions.

α_i = Appropriate mean coefficient of thermal expansion (Reference ASME code section III Appendix, 1977 Edition) from 70°F to indicated average temperature

In the case of an increase to the 10 percent power level, ΔL_1 is given by

$$\Delta L_1 = \alpha_1 B_1(T_1-70^\circ) + \alpha_2 B_2(T_2-70^\circ) + \alpha_3 B_3(T_3-70^\circ)$$

where

$T_1, T_2, T_3, B_1, B_2, B_3$, are defined on figure 2-25, and

α_1, α_2 and α_3 are defined the same as α_i

The actual values of, α, vary by approximately plus or minus 3 to 4 percent from the nominal thermal coefficient for a given material type. In the present analysis, the magnitude of variation can have a significant effect on the estimated force induced by a wedged part. In this analysis, a conservative approach was used. The reactor internals are assumed to have an α, that results in the largest growth; while the reactor vessel is assumed to have an α, that results in its smallest growth; thus, the analysis predicts the "absolute" minimum gap for the range of α. A statistical approach, (eg. using the SRSS method) would predict a more realistic and larger gap for each temperature condition.

2.4.2 PRESSURE EXPANSION

The Vessel extension due to pressure was calculated in accordance with the formulation in Roark's Formulae For Stress and Strain, Table XIII, Cases 1 and 2, 3rd Ed., p. 268 as

a) $\delta_{head} = \frac{.7PR^2}{2Et}$

b) $\delta_{cyl(i)} = \frac{.2PRL_i}{Et_i}$

The total expansion is then;

$$\delta_{r\ total} = \delta_{head} + \delta_{cyl(1)} + \delta_{cyl(2)} + \delta_{cyl(3)}$$

where:

P = operating or heat-up transient pressure, psia

R = Mean Radius of vessel or bottom vessel head, inches

L_i = Length of vessel of a specified thickness (figure 2.2-2), (in)

E_i, E = Modulus of elasticity, psi, corrected for average temperature for cylinder length L_i, and the modulus of elasticity for the head.

t_i, t = Vessel thickness, inches, for a given length of cylinder (see Figure 2.2-2) or the head thickness.

i = segment number of cylinder of length L_i and thickness

2.4.3 GAP SIZE CONSIDERING THERMAL GROWTH AND PRESSURE

The final gap for any temperature or pressure is then given by

$$\text{Gap} = \left(\left[\quad \right]^{a,b} - \Delta L + \delta_r \right) \text{ inches}$$

0583E:1

FIGURE 2.4-1 GAP SIZE VS. HEAT UP RATE

a,b

FIGURE 2.4-2 GAP SIZE VS PERCENT POWER

a,b

2.5 Operating Margins

The main areas of concern due to the load transmitted by the wedging action of parts are:

1) Hold down spring margin at the vessel ledge,
2) Energy absorber yield strength margin,
3) Vessel stress margins,
4) Radial key yield strength margin,
5) Core barrel yield and buckling margins.

2.5.1 Hold Down Spring Margin (Uplift Resistance)

The permanent set of CWE hold down springs was measured to be [ ]^{a,b} and the preload of the 304 SS hold down spring is [ ]^{a,b} lbs. (hot).

From static equilibrium of vertical mechanical and hydraulic forces in the lower internals, the reaction, R_V, at the vessel ledge during normal operation is given as,

$$R_V = F_S + F_C + F_W - F_L \qquad \text{(See Figure 2.5-1)}$$

(+)Down (-)Up

where

F_S = core barrel hold down spring force - lbs_f = [ ]^{a,b} (hot)

F_C = core reaction force on the lower core plates lbs_f and transmitted down to lower core support plate

The core reaction force, F_c, is calculated at a minimum value , in order to obtain a conservative hold down spring margin. Refer to Figure 2.5-1

$$F_{c(min)} = F_{c2} + F_{c1(min)} - F_{c3} - F_{c4}$$

Where:

F_{c1} = Fuel Assembly spring Load (min at BOL)-lbs_f

F_{c2} = Fuel Assembly weight-lbs_f

F_{c3} = Fuel Assembly Lift Force-lbs_f due to the drag force of the reactor coolant flow

F_{c4} = Fuel Assembly buoyancy-lbs_f

$F_{c(min)} = [\quad]^{a,b} lbs_f$

F_W = Lower internals weight (wet) - lbs = $[\quad]^{a,b} lbs_f$

F_L = Lower Internals Hydraulic (drag due to reactor coolant flow) lift force - lbs_f = $[\quad]^{a,b} lbs_f$ (up) on the lower core plate

Thus,

$$R_V = [\qquad\qquad]^{a,b} lbs_f$$

If a minimum value of $[\quad]^{a,b}$ lbs is maintained as margin against uncertainty, the reserve contact force at the vessel ledge becomes

$$R_V = [\qquad\qquad]^{a,b} lbs_f$$

Thus the induced load by the wedged parts must not exceed the above reserve contact force.

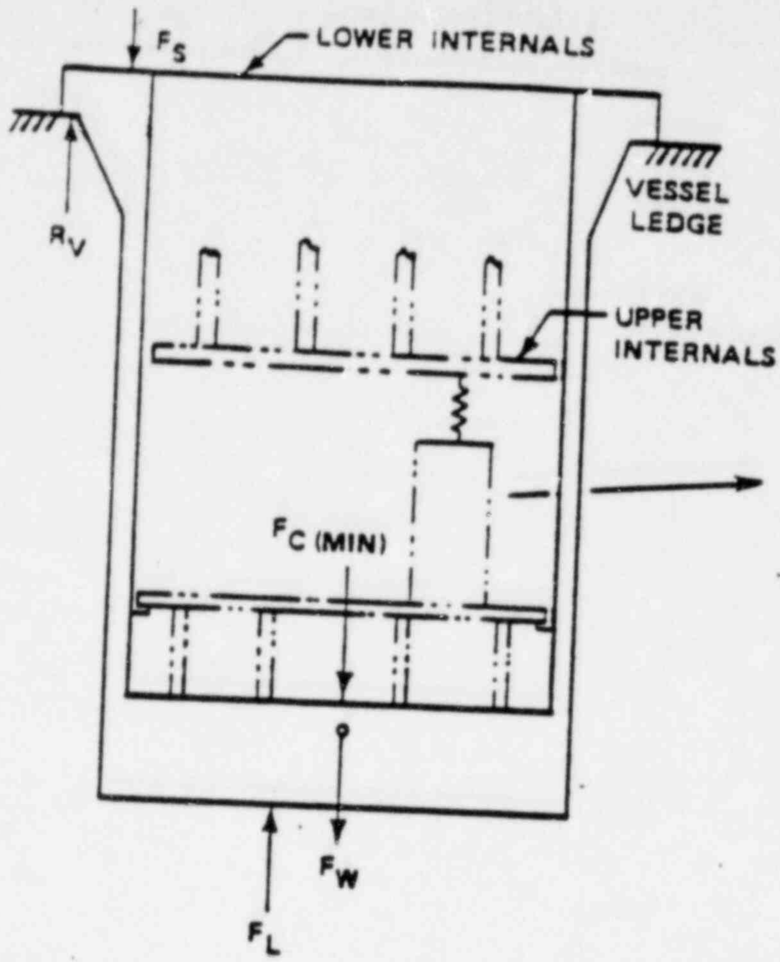

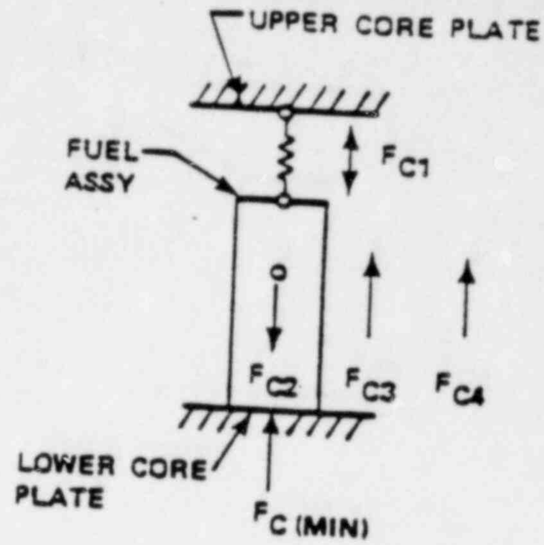

STATIC EQUILIBRIUM OF LOWER INTERNALS VERTICAL MECHANICAL AND HYDRAULIC FORCE COMPONENTS

WHERE:

$R_V = F_S + F_W + F_{C\,(MIN)} - F_L$

R_V = MIN REACTION FORCE AT VESSEL LEDGE – LBS.

F_S = MIN HOLD DOWN SPRING FORCE – LBS.

F_C = MIN FUEL ASSY REACTION FORCE – LBS. (TRANSMITTED FROM LOWER CORE PLATE)

F_W = LOWER INTERNALS BUOYANT WEIGHT – LBS.

F_L = LOWER INTERNALS HYD. LIFT FORCE – LBS.

STATIC EQUILIBRIUM OF FUEL ASSY FORCE COMPONENTS

WHERE:

$F_{C\,(MIN)} = F_{C1} + F_{C2} - F_{C3} - F_{C4}$

$F_{C\,(MIN)}$ = MINIMUM FUEL ASSY REACTION FORCE ON LOWER CORE PLATE – LBS.

F_{C1} = FUEL ASSY SPRING FORCE – LBS.

F_{C2} = FUEL ASSY WEIGHT – LBS.

F_{C3} = FUEL ASSY LIFT FORCE – LBS.

F_{C4} = FUEL ASSY BUOYANCE – LBS.

FIGURE 2.5-1 VERTICAL MECHANICAL AND HYDRAULIC FORCE COMPONENTS FOR LOWER INTERNALS

2.5.2 ENERGY ABSORBER YIELD STRENGTH MARGIN

An analysis was performed which shows that maintaining the load on the absorber below [ ]^{a,b} lbs does not cause yielding of the absorber; and the relaxation effects at temperature, caused by a deflection controlled load, will not reduce the energy absorption capability below acceptable margins. Even though it is believed that additional analysis would show that the absorber could be plastically deformed in excess of 0.1 inches without adversely affecting its energy absorption capability, the load induced in the energy absorber, due to wedging, is conservativaly limited to less than [ ]^{a,b} lbs., to prevent plastic deformation.

2.5.3 Vessel Margins

The stresses induced in the reactor pressure vessel by loads due to wedged loose parts were evaluated.

2.5.3.1 Vessel Bottom Head Margin

A conservative vessel load was calculated assuming that all loose parts become wedged at this location. The maximum postulated load of [ ]^{a,b} kips was assumed to be acting over a bearing area of [ ]^{a,b} square inches. The calculated maximum membrane stress intensity due to wedged part and normal operating loads is 24,543 psi, which compares favorably with the ASME code allowable of (1.5 S_m) 40,050 psi.

The calculated maximum primary plus secondary membrane plus bending stress intensity under the load is 45,536 psi, which compares favorably with the code allowable of (3 S_m) 80,100 psi.

The local Hertz contact stresses between the wedged part and the vessel cladding exceed the yield strength of the clad and some indenture will occur. Of all possible loose parts, the threaded portion of a bolt has the greatest potential for clad indentation due to the sharp corners of the threads. Assuming that a bolt head could be broken off from the bolt body, the bolt threads could be wedged against the vessel cladding. Conservatively assuming that the bolt is rigid, the maximum depth of indentation expected would be equal to the height of the thread profile. For ¼-20 UNC external threads this height is equal to 0.031 inches. The minimum clad thickness of the CWE vessel is [ ]^{a,b} inch. The minimum clad thickness minus the maximum expected indenture is equal to the present minimum required cladding thickness of [ ]^{a,b} inch. Therefore, the clad indentation which might be expected due to wedged loose parts is acceptable.

2.5.3.2 Vessel Core Block Margin

The loads for which the vessel was evaluated in this case were a radial load of [ ]^{a,b} kips and an axial load of [ ]^{a,b} kips, the same loads used for the radial key evaluation. The stresses due to the wedged parts loads were combined with the normal operating stresses and were shown to meet the ASME code requirements for stress intensity.

2.5.4 Radial Key Yield Strength Margin

The bottom of the lower internals assembly is restrained laterally by six uniformly spaced key (304 SS) which are mounted on pads on the lower support casting. The keyways are mounted on pads on the reactor vessel. Each key is 5.0 inch wide and has a nominal contact area with its keyway of 2.2 by 15.0 in. They side faces of keys are hardened by weld depositing Stellite No. 6 Alloy. The nominal total cold clearance of each key in the keyway is [ ]^{a,b} in. The keys are press fit laterally into a recess in the mounting pad on the core support casting. There are eight 0.875" dia. type 316 cold-worked stainless steel shear pins designed to take additional vertical loads and each key is clamped to the core support by ten

1.250-7-UNC type 316 cold-worked stainless steel cap screws.

2.5.4.1 Loads From Jamming the Key

The stresses in the radial key are calculated for the loads due to 26 bolt heads jammed in the radial gap between the key face and the clevis insert. It is conservatively assumed that the bolt heads become wedged cold and are crushed due to relative thermal expansion of the internals and vessel during plant heat up. Since the lower internals and lower vessel are at the inlet temperature during heat up, the relative radial expansion is due only to the different coefficients of thermal expansion of the internals and vessel. The calculated relative radial thermal expansion of the vessel and internals is [ ]^{a,b} inches. Conservatively assuming that the lower support structure and vessel are rigid, the radial load induced in the key is calculated for a bolt deformation of [ ]^{a,b} inches using equation (2.4) from Section 2.1. The resultant radial load in the key is equal to [ ]^{a,b} kips.

Since the relative axial expansion of the vessel and internals is approximately 0.500 inches, either the jammed bolts must slip or be at their maximum shear load capacity. Conservatively assuming the latter, the axial load in the key is calculated to be equal to one half of the radial load, or [ ]^{a,b} kips.

2.5.4.2 Model and Analysis

The radial key as shown in Figure 2.5-2 is modeled as a short built-in beam, its dimensions is conservatively calculated in Figure 2.5-2C. The major concern is in the root of the key.

a) tangential load = [ ]^{a,b} lb_f

$$\tau_{yx} = \left[\quad \right]^{a,b} = 450 \text{ psi}$$

$$\sigma_x = \frac{MC}{I_{zz}} = \left[\quad \right]^{a,b} = 1320 \text{ psi}$$

FIGURE 2.5-2 RADIAL KEY AND ITS MODEL

a,b

σ_x adjusted by stress concentration factor of 1.8 [2]

σ_x = 1320 x 1.8 = 2370 psi

b) Radial load = [ ] lb_f (compressive)

$\sigma_x = [\quad]^{a,b} = 1560$ psi

c) Axial load $= [\quad]^{a,b} lb_f$

$\tau_{xz} = [\quad]^{a,b} = 773$ psi

$\sigma_x = [\quad]^{a,b} = 952$ psi

The maximum stress intensity produced is 5,200 psi. In view of this relatively small magnitude and duration of this stress, safety is not a concern.

The next consideration is on the shear pins. Since the majority of vertical loads are taken by the frictional capacity in the press fit, approximately $[\quad]^{a,b} lb_f$, very little load is on the shear pins. The vertical load, $[\quad]^{a,b}$ lb, small in comparison with $[\quad]^{a,b} lb_f$, to make the press-fit assembly to slip. Thus, no safety problem in the shear pins.

2.5.5 Core Barrel Margin

The major concern on the core barrel is the compressive stresses created when one of the radial keys is jammed by the loose parts and, thus, axial thermal expansion of the core barrel is constrained during heat up.

2.5.5.1 Core Barrel Buckling Margin

The portion of the core barrel affected by the jamming of the radial key is conservatively modeled as shown in Figure 2.5-3. From [2], the buckling stress is given by

$$\sigma = \frac{1}{6} \frac{E}{1-W^2} \quad [(12\ (1-W^2)\ (\frac{t}{r})^2 + (\frac{\pi t}{b})^4\ ]^{\frac{1}{2}} + (\frac{\pi t}{6})^2$$

Substituting gives

$$\sigma = 610{,}000 \text{ psi}$$

Compressive stresses in core barrel

$$\sigma = \left[\qquad \right]^{a,b} = 1{,}840 \text{ psi}$$

Thus, the margin for buckling is very large.

a,b

FIGURE 2.5-3 CORE BARREL EFFECTIVE REGION

2.5.5.2 Core Barrel Flange Lifting Margin

Due to the worst possible jamming of loose parts on one radial key, an additional upward lifting force, F_u, of $[\quad]^{a,b}$ lb., could act on the core barrel flange. Since a minimum value of $[\quad]^{a,b}$ lbs should be maintained as a margin against uncertainty, and the additional uplifting force is acting on part of the core barrel flange. The equation is rewritten as:

$$\frac{R_v}{2\pi rt} = \frac{1}{2\pi rt}(F_s + F_w + F_c - F_L) - \frac{F_u}{\ell t}$$

where t = thickness in the radial direction of the spring-core barrel flange contact area.

ℓ = length of arc that uplifting force is acting

r = radius of core barrel

The criteria is that $R_v \geq [\quad]^{a,b}$ Assuming, ℓ, the length of the arc equals to the length of the support casting which radial key is mounted on plus the length of arc 15° radiated from the side of the casting, shown in the following schematic drawing, on each side:

$$\ell \doteq [\quad]^{a,b} + 2 \times [\quad]^{a,b} \times \tan 15°$$
$$\doteq 196.8''$$

which corresponds to $[\quad]^{a,b}$ radians

Simplify the above equation and substitute appropriate values.

$$R_V = F_S + F_W + F_C - F_u - \frac{2\pi}{2.56} F_u$$

$$= \Big[\qquad\qquad\qquad\qquad\qquad\qquad \Big]^{a,b}$$

$$= 114{,}770 > \big[\qquad \big]^{a,b}$$

Thus, the induced load by the jammed loose part does not exceed the above reserve contact force.

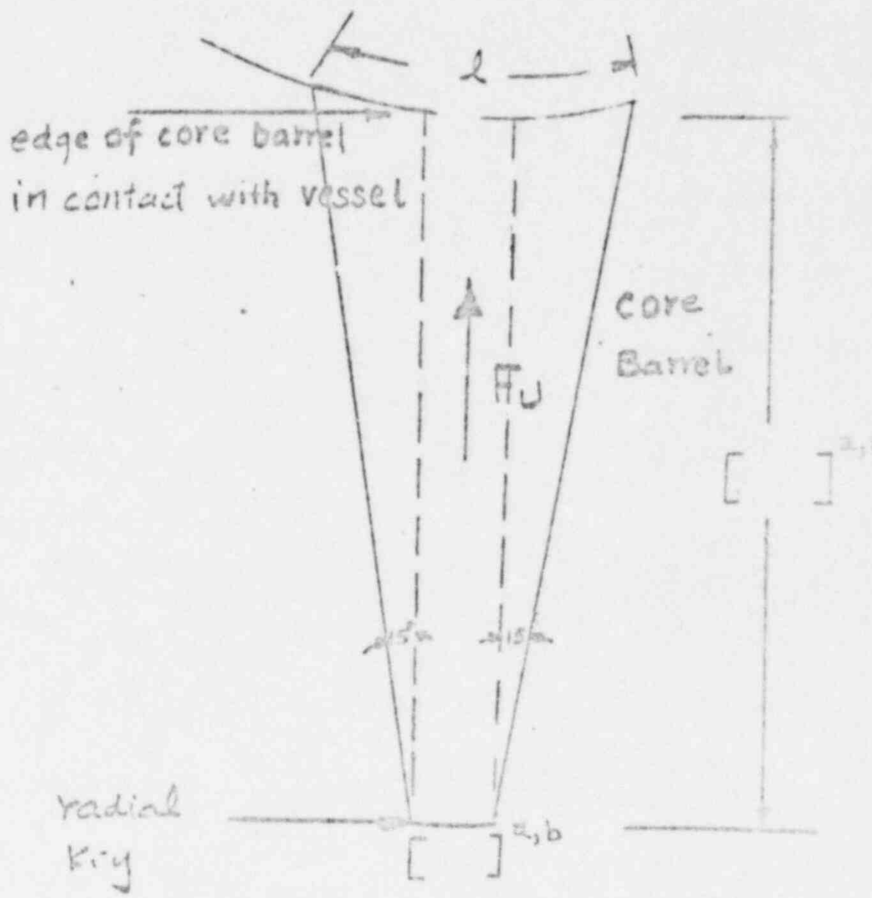

Schematic drawing of portion of the core barrel jamming acted upon.

2.6 Results of Wedged Part Analysis

The results of the analysis to predict the effects of loose parts wedged at the two postulated locations are summarized in this section.

2.6.1 Parts Wedged in Lower Radial Support

The analysis in the preceding sections determined that the case of 26 bolts wedged in a single radial key-clevis insert gap was not critical for any of the concerns listed in Section 2.0.

2.6.2 Parts Wedged Beneath Secondary Core Support

Due to the potentially complicated geometry of loose parts configurations in this location a more detailed study is required. The gap sizes at this location are presented for various heatup rates and pressures in Figure 2.4-1. Likewise, the gaps for various levels of power and pressures are presented in Figures 2.4-2.

Induced loads for various levels of potential loose part interference may be calculated using the stiffnesses of the loose parts as determined in Section 2.1 and the reactor internals and vessel system determined in Section 2.2. In order to facilitate this load calculation, plots of potential part interference versus load are made for 26 wedged bolt heads with varying constant wedging load components. This constant load component is the total load induced by wedged parts other than bolt heads. Thus for any loose part configuration and gap size, the potential induced load is found by calculating the constant load due to interfering nuts, washers and hinge fragments and then applying Figures 2.6-1 through 2.6-3 for the appropriate degree of bolt head interference. If there is no potential bolt head interference then the total load is equal to the constant value P_c.

FIGURE 2.6-1 LOAD VS INTERFERENCE

a,b

FIGURE 2.6-2 LOAD VS. INTERFERENCE

2.b

FIGURE 2.6-3 LOAD VS. INTERFERENCE

a,b

Assuming that all parts are potentially wedged in the gap between the secondary core support and inside vessel head, the resultant maximum potential load is evaluated for four assumptions regarding loose parts geometries. These four assumptions are listed as (A) through (D) below.

ASSUMPTIONS:

A) Part assemblies do not separate and do not stack.

B) Part assemblies do not separate but may stack.

C) Part assemblies separate but do not stack.

D) Part assemblies separate and stack.

An extensive study of possible loose part configurations for each assumption was performed. Figures 2.1-3 through 2.1-7 show some possible sub-configurations of single and stacked loose parts. The maximum loads due to loose parts are determined assuming that all the parts are wedged at this location in the worst combination of sub-configurations. Tables 2.6(A) and 2.6(B) show the maximum potential load calculated for worst case configurations analyzed for assumptions (A) and (B). The maximum loads are calculated in the following manner.

MAXIMUM LOAD CALCULATION FOR LOOSE PART SUB-CONFIGURATIONS

i) Assume nuts, washers and hinge fragments are at their maximum load capacity. This assumption is valid since these parts may sustain very low deflections elastically. Also, the cross-sectional area for these parts as shown in Figures 2.1-3 through 2.1-7 does not very drastically during deformation.

ii) For bolt head deformation, use the curves of Figures 2.6-1 through 2.6-3. These curves were generated based on changing bolt head cross sectional area, conservatively for 26 bolts, during bolt head deformation and the stiffness model of the reactor vessel internals. The value of δp on these curves is the original potential interference for a given gap size, or the total height of the stacked bolt head sub-configuration minus the gap size for which the load is to be determined (no potential interference is possible for negative values of δp). The value of Pc on the curves is the constant load component that exists for deforming nuts and washers.

TABLE 2.6(A)

LOOSE PART CONFIGURATION I
WORST CASE FOR ASSUMPTION (A)

SUB-CONFIGURATION	MAXIMUM NUMBER OF SUB-CONFIGURATIONS
B (Figure 2.1-3)	1
N (Figure 2.1-6)	22
O (Figure 2.1-6)	21

P_c = 1(21006) + 22(1734) = 59154 lb.

δ_p = 0.469 - [ ]^{a,b} = [ ]^{a,b} inch

P_{max} = [ ]^{a,b}

(Figures 2.5-1 and 2, Interpolating between P_c = [ ]^{a,b} and P_c = [ ]^{a,b} for P_c = [ ]^{a,b}

TABLE 2.6 (B)

LOOSE PART CONFIGURATION (II)
WORST CASE FOR ASSUMPTION (B)

SUB-CONFIGURATION	MAXIMUM NUMBER OF SUB-CONFIGURATIONS
L (Figure 2.1-5)	1

P_c = 98,641 lb.

δ_p = N/A

P_{max} = 98641 lb. < $\left[\quad \right]^{a,b}$ lb.

Since the assumptions (A) and (B) are valid, the maximum allowable load on the secondary core support [ ][a,b] is not violated. Since assumption (C) is bounded by assumption (A) then there is no potential problem if assumption (A) is valid. Assumption (D) however, shows that potential problems do exist if separated loose parts somehow stack up. This subject is discussed in Section 2.6.3.

2.6.3 Discussion of Potential Problems and Recommended Operating Procedure

From Sections 2.6.1 and 2.6.2 the only potential problem exists for loose parts wedged beneath the secondary core support and stacked according to Assumption (D). The source of this problem lies in the fact that separated loose part assemblies are assumed to stack up in the worst possible conceivable manner. Therefore, the bounding stacking configurations are described in this section in order to clarify the sources of potential problems. The worst case loose part configurations are described and the method of potential interference load calculation for each case is presented.

2.6.3.1 Loose Part Configuration ID

This loose part configuration is a combination of the sub-configurations shown in Figures 2.1-3 through 2.1-7. The maximum number of each sub-configuration is based upon the assumption of 21 assemblies (latest count). The maximum load for each sub-configuration is determined in the following manner.

Maximum Load Calculation for Loose Part Sub-Configurations

i) Assume nuts, washers and hinge fragments are at their maximum load capacity. This assumption is valid since these parts may sustain very low deflections elastically. Also, the cross-sectional area for these parts as shown in Figures 2.1-3 through 2.1-7 does not vary drastically during deformation.

ii) For bolt head deformation, use the curves of Figures 2.6-1 through 2.6-3. These curves were generated for 26 bolts based on changing bolt head cross sectional area during bolt head deformation and the stiffness model of the reactor vessel and internals. The value of δp on these curves is the original potential interference for a given gap size, or the total height of the stacked bolt head sub-configuration minus the gap size for which the load is to be determined (no potential interference is possible for negative values of δp). The value of Pc on the curves is the constant load component that exists for deforming nuts and washers.

Table 2.6.4-1 lists the sub-configurations that make up Configuration ..

Table 2.6.4-1

Sub-Configuration	Maximum Number of Sub-Configurations
A	21
C	11
B	1

Thus, the value of Pc for Configuration ID may be calculated.

$$P_c = 11(8382) + (1)21006 = 113,208 \text{ lb.}$$

Potential interference for a gap size of $[\quad]^{a,b}$ inch is calculated for 100°F/hr. heat up rate and 1000 psi.

$$\delta p = .5313 - [\quad]^{a,b} = [\quad]^{a,b} \text{inch.}$$

Using the curve of Figure 2.6-2 for P_c = 125,000 lb. and δp = 0.0863 inch shows that the total load is equal to approximately 220 kips. From the same curve it is seen that the interference for the allowable load of [ ]^{a,b} kips is approximately [ ]^{a,b} inches. The gap size that would produce this level of interference is [ ]^{a,b} which is greater than the height of sub-configurations (B) and (C). Therefore, a different procedure must be employed in order to determine the allowable gap size for configuration ID.

Calculation of Minimum Gap Size For Configuration ID

The most direct procedure is to generate a plot of load versus interference. In order to determine the coordinates of points on the plot, the following procedure is used.

1) Assume that sub-configurations (B) and (C) behave elastically (valid if deformations of these sub-configurations are small).

2) Determine the linear load-deflection relationship for sub-configurations (B) and (C).

3) Determine the load-interference relationship for configuration ID using the wedged part and internals - vessel system stiffnesses.

Determination of Data Points for Load-
Interference Plot for Configuration ID

For interferences of less than [ ]^{a,b} inch, the plot for P_c = 0 given in Figure 2.6-1 may be used. This is true because sub-configurations (B) and (C) are not loaded for these levels of interference. For interferences greater than [ ]^{a,b} an additional stiffness due to sub-configurations (B) and (C) is acting. Thus the load-interference plot will not be continuous.

The equivalent linear stiffnesses for sub-configurations (B) and (C) are calculated assuming an elastic modulus, $E = 25.4 \times 10^6$ psi.

Sub - Configuration	Area, A (in^2)	Height, L (in)	$K_{eq} = \frac{AE}{L}$ ($^{Lb}/in$)
B	0.3308	0.500	16.805×10^6
C	0.132	0.500	6.706×10^6

Since the sub-configuration (B) and (C) equivalent springs act in parallel, the effective spring constant is the sum of the equivalent spring rates.

$$K_{effective} = \left\{16.805 + 11\times(6.706)\right\} \times 10^6 \text{ lb/in}$$

$$= 90.57 \times 10^6 \text{ lb/in}$$

The non-linear load-deflection relationship of the bolt head is given by equation (2.4) of Section 2.1.1.

The resultant load-interference plot for configuration ID is shown in Figure 2.6-4. From this figure it is seen that for an allowable load of [ ]^{a,b} kips, the interference is equal to [ ]^{a,b} inch.

Therefore, the minimum allowable gap, G_A, assuming that configuration ID may occur is calculated.

$$G_A = [\quad]^{a,b} \text{ inch}$$

$$G_A = [\quad]^{a,b} \text{ inch}$$

FIGURE 2.6-4 LOAD VS. INTERFERENCE

a,b

2.6.3.2 Loose Part Configuration IID

This loose part configuration is also a combination of the sub-configurations shown in Figures 2.1-3 through 2.1-7. Again assuming that parts due to all 21 assemblies are present the sub-configurations that make up Configuration IID are listed in Table 2.6.4-2.

Table 2.6.4-2

Sub-Configuration	Maximum Number of Sub-Configurations
D	21
E	2
B	1
C	11

Thus, the value of Pc for Configuration IID may be calculated.

$$Pc = 21(1778) + 2(20447) + 1(21006) + 11(8382)$$

$$Pc = 191,440 \text{ lb.}$$

CALCULATION OF MINIMUM ALLOWABLE GAP SIZE FOR CONFIGURATION IID TO MAINTAIN MINIMUM CORE BARREL TO VESSEL LEDGE LOAD

The minimum allowable gap size assuming configuration IID may occur is calculated by accounting for the internals and vessel system and wedged part flexibilities.

It is known that due to the large degree of deformation that occurs in sub-configuration (D). Therefore, this sub-configuration is at its ultimate load carrying capability. Sub-configurations (E), (B), and (C), however, will have limited deformations and may be assumed to be elastic for an initial iteration. The equivalent spring constants for each sub-configuration is calculated assuming an elastic modulus, $E = 25.4 \times 10^6$ psi.

Sub-configuration	Area, A (in^2)	Height, L (in)	$K_{EQ} = \frac{AE}{L}$ (lb/in)
B	0.3308	0.500	16.805×10^6
C	0.132	0.500	6.706×10^6
E	0.322	0.500	16.358×10^6

Since the sub-configuration equivalent springs act in parallel, the effective spring constant is the sum of the equivalent spring rates.

$$K_{effective} = 16.805 + 2(16.358) + 11(6.706) \quad \times 10^6 \text{ lb/in}$$

$$= 123.29 \times 10^6 \text{ lb/in}$$

The load in the effective spring, P_K, is equal to the maximum allowable load minus the constant load due to sub-configuration (D), P_{c1}.

$P_{c1} = 21(1778) = 37,338$ lb.

$P_K = [\quad]^{a,b} - 37,338)$ lb $= [\quad]^{a,b}$ lb.

The deflection of the effective spring, δ_K, is equal to the spring load divided by the spring rate.

$$\delta_K = \frac{[\quad]^{a,b}}{123.29 \times 10^6} \text{ inch}$$

$$\delta_K = [\quad]^{a,b} \text{ inch}$$

Check assumption of elastic deformation in sub-configurations (B), (C) and (E):

$P_E = 16.358 \times 10^6 \left[\quad \right]^{a,b} \text{lb} = \left[\quad \right]^{a,b} \text{lb.}$

since $\left[\quad \right]^{a,b} < 20{,}447$ sub-configuration (E) deforms elastically

$P_B = 16.805 \times 10^6 \left[\quad \right]^{a,b} \text{lb} = \left[\quad \right]^{a,b} \text{lb.}$

since $\left[\quad \right]^{a,b} < 21{,}006$ sub-configuration (B) deforms elastically

$P_C = 6.706 \times 10^6 \left[\quad \right]^{a,b} \text{lb} = \left[\quad \right]^{a,b} \text{lb.}$

since $\left[\quad \right]^{a,b} < 8382$ sub-configuration (C) deforms elastically

Therefore, the assumption of elastic deformation in sub-configurations (B) (C) and (E) is valid.

The deformation of the internals and vessel systems, δ_s, due to the maximum allowable load must be added to the deformation of the wedged parts in order to determine the minimum allowable gap size.

$\delta_s = \left[\quad \right]^{a,b} \text{inch}$

$\delta_s = \left[\quad \right]^{a,b} \text{inch}$

Thus the allowable interference, δ_d, is equal to the deformation of the internals and vessel system plus the wedged part deformation at the maximum allowable load.

$\delta_D = \delta_K + \delta_s$

$\delta_D = \left[\quad \right]^{a,b} \text{inch}$

$\delta_D = \left[\quad \right]^{a,b}$

The minimum gap size, G_A, is equal to the minimum wedged part configuration height minus the allowable interference.

$$G_A = (0.500 - [\qquad]^{a,b} \text{ inch} = [\qquad]^{a,b} \text{ inch}$$

2.6.3.3 Discussion of Loose Part Configurations

From the calculations of Sections 2.6.3.1 and 2.6.3.2 it is seen that the loose parts configuration that results in the most restrictive gap size is configuration IID. Although configuration ID predicts essentially the same allowable gap size as configuration IID, the analysis of configuration ID is based upon load-interference plots generated for 26 wedged bolt heads and is therefore overly conserva[illegible]. The analysis, however, is useful in that it shows that configuration ID is not as limiting as configuration IID.

Although there is no basis for determining that configuration IID absolutely may not occur, it is statistically unlikely that all 21 bolts would be standing on head and all nuts and washers arranged in vertical stacks. Assuming that only half (11) of the bolts are standing on head reduces the maximum possible load due to configuration IID by 17,780 lb to a value of 173,660 lb. Assuming that the stacking of nuts and washers may be precluded results in a maximum load of 37,338 lb.

The consequence of configuration IID occuring in its worst form is that the reaction at the vessel ledge-core barrel flange interface is reduced to a value of $[\qquad]^{a,b}$ lb or 65.6 percent of the recommended minimum value to preclude undesirable flow-induced vibrations.

2.6.4 Recommended Operating Procedure

Based on the results of Section 2.6.3, it is recommended that the plant be operated in such a manner as to not violate a minimum gap of $[\qquad]^{a,b}$ inch between the secondary core support and inside vessel head. In order to investigate any restrictions in heat up rate or power escallation, the minimum allowable gap size is plotted as shown in Figures 2.7-1 and 2.7-2. Figure 2.7-2 shows that no restriction in power level is required for any of the plotted pressures. Possible limitations on heat up rate are discussed in Section 2.6.4.1.

2.6.4.1 Effect of loose Parts on Heat Up Procedures

From the analysis of Sections 2.3 and 2.4 it may be shown that heat up from 70°F to 450°F at a constant rate of 100°F per hour results in a zero pressure gap of $[\quad]^{a,b}$ inches at 450°F. Therefore the minimum gap requirement of $[\quad]^{a,b}$ inches is not violated for heat up rates up to 100°F per hour at temperatures from 70°F to 450°F.

Heat up from 450°F to 550°F, however, may cause the minimum recommended gap to be violated for certain heat up rate and pressure combinations, as shown in Figure 2.7-1. The minimum pressure for given temperatures is obtained from Reference [3] and is shown in Table 2.6.4-1.

TABLE 2.6.4-1

Temperature (°F)	Minimum Pressure (PSIG)
350	350
400	480
450	660
500	1060
550	1540

Using the temperature-pressure relations in Table 2.6.4-1, the minimum gap size may be bounded for a 60°F per hour heat up rate. Since it has been shown that the minimum gap requirement is not violated for temperatures up to 450°F at heat up rates up to 100°F per hour, the range of temperature to be examined is from 450°F to 550°F. The vessel stiffness is evaluated for the temperature distribution that exists at 450°F. The vessel expansion due to pressure, G_p, for this case is

$$G_p = \left[\qquad \right]^{a,b} P \text{ inch}$$

where P is the vessel pressure (psig)

The minimum gap occurs at the end of the heat up ramp when thermal lags in the vessel are the greatest. The zero pressure gap for heat up to 550°F at a rate of 60°F per hour is $[\quad]^{a,b}$ inch. Assuming the stiffest vessel (at 450°F) and minimum pressure (at 450°F) the minimum vessel expansion due to pressure is equal to $[\quad]^{a,b}$ inches. The minimum gap, G_{min}, corrected for the vessel expansion due to pressure is

$$G_{min} = [\qquad\qquad]^{a,b} \text{ inch}$$

Thus, the minimum gap that occurs for the temperature range from 450°F to 550°F during a 60°F per hour heat up rate does not exceed the minimum gap requirement if the minimum pressures given in Table 2.6.5-1 are satisfied.

FIGURE 2.7-1 HEAT UP RATE VS. GAP SIZE

a,b

FIGURE 2.7-2 PERCENT POWER VS. GAP SIZE

a,b

2.7 Summary Wedged Part Effects

A comprehensive review of the lower internals package was performed in order to determine areas where objects could lodge and present possible concerns. Two areas were determined as potential wedging locations that could cause concerns during heat-up and operation of the plant. These locations, shown in Figure 2-1 are the gap between the secondary core support plate and the vessel bottom head and the radial gap between the radial key and clevis insert.

The effects of the postulated wedging were evaluated for three items of concern:

1) Loads induced in core support structures during plant heat-up and power escalation.

2) Minimum core barrel flange to vessel ledge load to preclude undesireable flow-induced vibrations.

3) Loads induced in reactor pressure vessel.

The results of the three evaluations performed are summarized in Sections 2.7.1 through 2.7.3.

2.7.1 Effects of Loads Induced in Core Support Structures Due to Wedged Parts

The effects of loads induced on core support structures due to parts wedged at the two postulated locations are summarized in Sections 2.7.1.1 and 2.7.1.2.

2.7.1.1 Parts Wedged in Lower Radial Support

The case of 26 loose bolts wedged between a single radial key and clevis insert was evaluated. The postulated wedging condition was determined to induce a radial load of [ ]^{a,b} kips and an axial (vertical) load of [ ]^{a,b} kips on the radial key. The maximum stress intensity induced in the radial key was determined to be 5200 psi. The factor of safety for an allowable stress intensity of 48,600 psi (3 S_m) is 9.3.

In addition to the radial key, the stresses induced in the core barrel were evaluated. The compressive stress in the barrel due to the wedged part was determined to be 1840 psi. The factor of safety for an allowable stress intensity of 48,600 psi (3 S_m) is 26.4. Additionally, the core barrel was analyzed for potential buckling. The analysis showed that this possibility is precluded.

2.7.1.2 Parts Wedged Beneath Secondary Core Support Structure

The load path through the core support structures due to parts wedged in this location is shown in Figure 2.2-1. Analysis of the affected structures shows that the critical load for structural integrity is [ ]^{a,b} kips based on yielding of an individual column of the energy absorber. This load is greater than the [ ]^{a,b} kip critical load determined for maintaining minimum core barrel flange to vessel ledge load.

2.7.2 Minimum Core Barrel Flange to Vessel Ledge Load

The core barrel flange to vessel ledge load was determined for normal hot and cold conditions based on as-built drawing dimensions and operating loads. The hot load was determined to be [ ]^{a,b} kips. The effects of wedged parts in the two postulated locations on the ability to maintain the minimum allowable load of [ ]^{a,b} kips were determined. The results are summarized in Sections 2.7.2.1 and 2.7.2.2.

2.7.2.1 Parts Wedged in Lower Radial Support

Since the compressive load in the core barrel is not uniform throughout all sections for this load case, the minimum load per circumferential inch at the core barrel flange-vessel ledge interface at the critical section is the governing criteria. The analysis based on a vertical compressive load of [ ]^{a,b} kips and an effective core barrel region showed that the minimum requirement is not exceeded.

2.7.2.2 Parts Wedged Beneath Secondary Core Support Structure

For this case it was postulated that all parts were potentially wedged in this location. The gap size for various heat-up rates and power levels at various pressures was determined based on as-built drawing dimensions and operating loads. The results are shown graphically in Figures 2.4-1 and 2.4-2. A comprehensive stiffness model of the vessel, reactor internals and postulated loose parts was used to determine the load induced by various degrees of interference due to loose parts. The model is shown in Figure 2.2-2.

Four assumptions regarding possible geometries of loose parts wedged at this location were made and a comprehensive study was performed in order to determine the maximum possible load for each assumption.

The assumptions and maximum loads are presented in Table 2.7-1. Since the maximum allowable load is [ ]^{a,b} kips, only assumption (D) indicated that a potential problem existed. A critical gap size was determined based on this assumption and was plotted on Figures 2.7-1 and 2.7-2 as the dividing line between acceptable and unaccpetable gap sizes.

TABLE 2.7-1 POTENTIAL LOAD ON SECONDARY CORE SUPPORT DUE TO WEDGED PARTS

ASSUMPTION	MAXIMUM POTENTIAL LOAD ON SECONDARY CORE SUPPORT PLATE (KIPS)	RECOMMENDED OPERATING PROCEDURE
A	107.4	None
B	98.6	None
C	$\geq$ 107.4	None
D	(See Section 2.6.3)	(See Section 2.6.4)

ASSUMPTIONS:

A) Part assemblies do not separate and do not stack.

B) Part assemblies do not separate but may stack.

C) Part assemblies separate but do not stack.

D) Part assemblies separate and stack.

2.7.3 Loads Induced in Reactor Pressure Vessel

The effect of loads induced in the reactor pressure vessel due to wedged loose parts in the two postulated locations were evaluated.

2.7.3.1 Parts Wedged in Lower Radial Support

The stresses induced in the vessel due to the radial load of [ ]^{a,b} kips and axial load of [ ]^{a,b} kips were calculated and combined with normal operating stresses. The resulting vessel stress intensities do not exceed allowable values.

2.7.3.2 Parts Wedged Beneath Secondary Core Support Structure

The stresses induced in the vessel due to the load of [ ]^{a,b} kips distributed over an area of [ ]^{a,b} square inches at the inside vessel bottom head were calculated and combined with normal operating stresses. The resulting vessel stress intensities do not exceed allowable values.

2.7.3.3 Local Stresses in Vessel Cladding

The potential for cladding indentation was considered to be greatest for a bolt body wedged in such a way that the bolt threads contact the vessel cladding. The maximum postulated depth of indentation was such that the present minimum clad thickness requirement is not violated.

3.0 INTRODUCTION IMPACT EFFECTS

The following is a summary of the work completed to evaluate the potential damage that may result due to the loose parts impacting against the core barrel, thermal shield flexures and bottom mounted instrumentation vessel tubes. These targets are the most sensitive structures for impact loads in the flowpath of the missile from the pump to the bottom of the reactor vessel. The current work is based on a conservative estimate of the damage that could result from the impacting of the largest loose part found in the vessel. The analysis considers both the potential for penetration by the parts, as well as overall structure damage.

3.1 DEFINITION OF MISSILE

3.1.1 MISSILE GEOMETRY

The largest loose part is the bolt-washer-nut assembly. The part is shown in Figure 3-1a. The mass of the assembly is

$$0.582 \times 10^{-3} \quad \frac{\text{lb. sec}^2}{\text{ft.}}$$

based on the weight of 304 stainless steel.

A second missile is the largest segment of a broken hinge. The segment is the No. 4 piece in Figure 3-1b.

3.1.2 MISSILE VELOCITY

The velocity of the missile was assumed to be equal to the velocity of the fluid flow at the location of the target. The flow rate considered was for normal operation mechanical design flow. The velocities, from POLAC Run APVQBMJ (4-2-82), at specific areas are:

1. Inlet Nozzle [ ][a,b]

2. Thermal shield flexure [ ][d,b]

3. Instrument tubes [ ][a,b]

The velocity used for the missiles is considered conservative. These velocities are achievable if the missile is in the flow for the distance of approximately 20 ft. without impacting or rubbing against the sides of the pipe or thermal shield annulus walls during flow.

3.1.3 MISSILE ENERGY

The energy of the missile upon impact is given by the equation:

$$E = (\tfrac{1}{2})mV^2$$

The E for the defined missiles are:

1. largest plate missile

a) At Inlet E = 1.76 lb. ft.
b) At Flexure E = 0.347 lb. ft.
c) At Tube E = 0.693 lb. ft.

2. Bolt Missile

a) At Inlet E = 1.88 lb. ft.
b) At Flexure E = 0.370 lb. ft.
c) At Tube E = 0.738 lb. ft.

3.2 TARGET GEOMETRY

As previously discussed, three potential targets have been defined that constitute the most sensitive parts in the flow path of the missile from the pump to the bottom of the reactor vessel. The targets are:

a) core barrel;
b) thermal shield flexure;
c) instrument tube.

In all cases the material properties used in the evaluation are those for the appropriate target material at 650°F.

The core barrel and analysis model are shown on Figures 3-2a and b; the flexure and analysis model are shown on Figures 3-3a and b; and the instrument tube and analysis models are on Figures 3-4a and b.

3.3 METHODS OF ANALYSIS FOR MISSILE IMPACT

The two major considerations for evaluating missile impact are limitations of local damage and of overall response of the target structural element. Local damage may include penetration or punching shear in the region of impact on the structure. Overall response includes bending and reaction shear in the structure.

Criteria for penetration and local punching shear are discussed in Section 3.3.1 and the evaluation of overall response is described in Section 3.3.2. The prediction of overall response is generally based on energy/momentum balance. The criteria of acceptance is that the target can absorb the impact energy without deformation that would impair the operation of the plant.

In all cases considered, the impact is assumed at an angle of strike normal to the target. The angle of strike has a substantial influence on the penetration depth and the energy that must be absorbed by the target. In some cases, such as the instrument penetrations, the probable angle of strike would appear to be substantially greater than 20°. An impact at 20° has approximately 12 percent less energy than a normal strike, and an impact at 30° is 25 percent less than the normal strike energy. Considering the actual flow conditions in the reactor, the normal strike assumption is considered very conservative.

3.3.1 LOCAL IMPACT EFFECT

Two local impact effects have been considered for the targets. The effects are:

1) Punching shear; and,

2) Penetration (denting)

The two are discussed in Sections 3.3.1.1 and 3.3.1.2 respectively.

3.3.1.1 PUNCHING SHEAR

The minimum energy required for the missile to punch out a plug of plate in shear was also evaluated. The failure mechanism is as shown on Figure 3-5. The minimum energy required is given by:

$$W_s = \int_o^h S_s R_F (d-x)\, dx$$

Where: x is the distance traveled through the plate;

R_F is the perimeter of the missile;

S_s is the yield of the target material in shear; and,

d is the plate thickness.

Evaluating the integral gives:

$$W_s = \frac{S_s R_F d^2}{2}$$

The value of S_s equal to one half the minimum yield stress at 650°.

The potential for perforation is given by the ratio:

$R_S = E_M/W_S$; where E_M is the kinetic energy of the missile.

Table 3-2 provides a summary of the R_S calculated for the various missile and target combinations.

TABLE 3-1

PERFORATION BY PUNCHING SHEAR

Missile	Target	W_S (lb.Ft.)	R_S
Lg. Plate	Core Barrel	1000	0.00088
Lg. Plate	Flexure	27	0.0064
Lg. Plate	Inst. Tube	94.5	0.0037
Bolt Assembly	Core Barrel	1280	0.0007
Bolt Assembly	Flexure	35.6	0.0052
Bolt Assembly	Inst. Tube	121	0.0031

Based on Table 3-1 results, the potential for perforation by punching shear is really negligible. The minimum factor of safety is 182.

3.3.1.2 PENETRATION (DENTING OF THE TARGET)

Conservative method is used to estimate an upper bound of the potential denting caused by the missile impact, the method utilizes the postulated failure mode in punching shear discussed in Section 3.3.1.1. The movement of the plug for a specified impact energy is estimated from the eqn.

$$E = \int_0^x S_S R_F (h-x)\, dx$$

Where x is the movement of the plug or the magnitude of the dent. S_S, R_F, and d are the same as in Section 3.3.1.1.

Integrating gives the energy required for the plug to move an amount X as:

$$E = S_S R_F \left(dx - \frac{x^2}{2}\right) + C$$

Using the initial condition that when E = 0 and x = 0, that C must equal 0; the equation for X is given by:

$$X^2 - 2dx + \frac{2E}{S_S R_F} = 0$$

$$X = \frac{2d - \sqrt{4d^2 - \frac{8E}{S_S R_F}}}{2}$$

The value of X estimated for various missile and target combinations is summarized on Table 3-2.

TABLE 3-2

POTENTIAL PENETRATION (DENT)

Missile	Target	Punching Shear Assumption
Lg. Plate	Core Barrel	0.001"
Lg. Plate	Flexure	0.001"
Lg. Plate	Inst. Tube	0.001"
Bolt Assembly	Core Barrel	0.0008"
Bolt Assembly	Flexure	0.001"
Bolt Assembly	Inst. Tube	0.0008"

As indicated in Table 3-2, the predicted dent is quite small. However, as previously stated, it is believed that the actual values would be much lower than the predicted values because:

1) They neglect that a minimum missile energy is required prior to initiation of denting or penetration; and

2) they neglect the energy dissipated in deformation of the target in regions not immediately under the missile, that will occur.

3.3.2 OVERALL STRUCTURE RESPONSE EFFECTS

In order to evaluate the overall response of the target structures for missile impact, the type of impact must be classified as either "hard" or "soft". The softness of a given impact is obviously relative, but in general, soft impact is characterized by significant local deformation of missile or target in the region of impact; while local deformation under hard impact is neglected. For soft impact, the deformation characteristics of the missile or target are used to develope an applied force time history, and the analysis of the structure is carried out as for an impulse load. In the case of hard impact, energy and momentum balance techniques are used to predict maximum response.

While the conditions of hard impact rarely exist in "real" life, the method is conservative with respect to predicting overall structure response and potential damage, because it neglects the energy absorption through local deformations.

The evaluation for potential damage was performed using the conservative assumption of hard impact.

Conservation of momentum and energy are used to determine the the portion of the kinetic energy of the missile that is transmitted to the structure to be absorbed as strain energy.

Conservation of momentum for Impact of two masses is:

$$M_1V_o = M_1V_1 + M_eV_2; \text{ and}$$

Conservation of energy is:

$$1/2\ M_1V_o^2 = 1/2M_1V_1^2 + 1/2M_eV_2^2$$

Where:

M_1 = Missile mass;
M_e = Target effective mass;
V_o = Velocity of missile before impact;
V_1 = Velocity of missile after impact;
V_2 = Velocity of missile after impact;

An additional equation can be written for the coefficient of restitution:

$$e = \frac{V_2 - V_1}{V_o}$$

0583E:1

Solving the equation for e for V_1, and substituting into the momentum equation yields the expression for post-impact target and missile velocity as:

$$V_2 = \frac{\frac{M_1}{M_e}}{1 + \frac{M_1}{M_e}} V_o (1+e) \quad ; \text{ and}$$

$$V_1 = \frac{\frac{M_1}{M_e} - e}{1 + \frac{M_1}{M_e}} V_o$$

For $M_1/M_e > e$ the missile velocity is positive after impact and the missile will move toward the target. Thus, the kinetic energy of the missile after impact must be absorbed by the target, in addition to the kinetic energy imparted to it during initial impact.

The energy to be absorbed by the target is then:

$$E = 1/2\, M_e V_2^2 \,, \quad \text{for} \quad \frac{M_1}{M_e} \leq e \;;$$

or

$$E = 1/2\, M_1 V_1^2 + 1/2\, M_e V_2^2 \,, \quad \text{for} \; \frac{M_1}{M_e} > e \,.$$

From the equations for velocities and the energy to be absorbed in structure strain energy, several observations are noteworthy:

1) An underestimation of target mass results in a conservative estimation of energy transmitted to the structure;

0583E:1

2) The upper bound of energy absorbed by the structure is when the target mass is assumed equal to zero (0), the upper bound energy is equal to the total kinetic energy of the missile at impact ($E = 1/2\ M_1 V_o^2$); and

3) The assumption that e = 1, or a perfectly elastic impact occurs, although unrealistic, is always conservative for estimating structural damage to the target.

3.3.2.1 Target Effective Mass

The effective mass of the target when a missile strikes a concentrated mass is obviously the total target mass. However, in the case of a distributed mass structure, the inertial resistance of the structure is actually a variable, changing during response and is dependent on the magnitude and duration of the applied loads.

Typically for impact evaluation, the effective mass (M_e) is that fraction of total structure mass determined based on the assumed static deformed shape of the structure due to the applied impact force. The equivalent mass is derived to maintain equality of kinetic energy with the real system.

$$M_e = m\ \phi(X)\ ^2dx$$

where m = mass per unit length; and,

$\phi(X)$ = assumed deflected shape.

In this regard, it is necessary to predict in advance whether the response will be elastic, elasto-plastic or plastic, because the deformed shape varies accordingly, as illustrated in figure 3-6. Table 3-4 provides values for M_e for some typical structural shapes for the elastic and plastic assumption. In some cases, to accurately define the M_e, an iterative procedure is required.

The M_e predicted by the above method generally participates in the final response of the structure. However, it may not be effective during the time of impact when energy is being transfered from the missile to the target. A structure subjected to an intense load for a very short duration will respond during impact only in the immediate area of the load, such that only a small portion of the structure mass participates in the energy transfer between missile and structure. If the impact results in a less intense load applied over a longer duration, then a greater portion of the structure mass will participate in the energy transfer. It is suggested in Ref. 9 that the minimum target effective mass is that included in an region within "d/2" of the periphery of the impact surface. The value of "d" is the thickness of the target in the direction of impact. This minimum mass must move if the structure as a whole is to deform. As discussed in section 3.3.1 failure within this area is governed by peforation or punching shear which have previously been shown to be a negligible possibility.

The actual determination of the mass is highly dependent on the geometry and elastic and plastic characteristics of both the missile and target. However, it can be bounded based on the duration of the time the force acts between the bodies. By assuming the missile remains elastic and the target is rigid, upon impact, a compressive stress wave propagates from the point of contact towards the free end of the missile. At the free end of the missile, the stress wave is reflected causing an expansion wave to return to the contact surface, such that the missile rebounds at the impact velocity. The impact time (t_d) is[10]

$$t_d = 2L/C$$

Table 3-4

EFFECTIVE MASS (M_e)

Beam Type	Elastic	Plastic
Simple-Simple Span Center Concentrated Load	0.494M	0.333M
Fixed-Fixed Span Center Concentrated Load	0.383M	0.333M
Cantilever Span Concentrated Load At Free End	0.243M	0.333M

M = Total Mass of Beam

From Reference 8

0583E:1

The force during impact is given by

$$P = \alpha C V_0$$

Where

P = Contact pressure (psi)

α = mass density of missile ($lb\text{-}sec^2/in^4$)

C = Speed of sound in missile (183688 in/sec)

V_0 = Impact velocity (in/sec)

L = Length of missile (in)

Thus the force time history applied to the target is a rectangular impulse load of constant magnitude for a duration of t_d. The value of t_d for a missile of length .75 inches is then

$$t_d = \frac{2L}{C} = 8.1 \times 10^{-6} \text{ sec}$$

The ability to mobilize the effective mass of the static deformed shape, (1st mode of structure), can be evaluated based on the response of the structure to a rectangular pulse force time history. The response in each mode of vibration for a uniform beam is[11]

$$X_n = \frac{\int_0^b p(x)\phi_n(x)dx}{\omega_n^2 \, m \, {}_0^{b} \, \phi_n^2 \, (x)dx} \, (DLF)$$

or

$$X_n = B \, (DLF)$$

Where:

DLF = Dynamic Load Factor

$\phi_n(x)$ = normalized shape of mode n

$p(x)$ = load as function of x

ω_n = circular frequency

m = mass per unit length

b = length of beam

The value B for a given mode is a constant and for simple shapes such as fixed - fixed beams and cantilever beams will be smaller for the higher modes than for the fundamental mode.

Figure 3-7 shows the Dynamic Load Factor (DLF) for a rectangular pulse load as a function of t_d divided by the period of vibration (T_1) of the structure. From this figure it is seen that for t_d/T_1 ratios greater than 0.5, where T_1 is the period of the first mode, the predominent response will be in the first mode, or the assumption for target mass based on the static deformed shape is valid. Conversely, for t_d/T_1 ratio less than 0.08, even if the term B for the first mode was two times that for the higher modes, the higher mode response could tend to dominate the total response; thus, the effective target mass assumption based on the minimum mass in the region of impact would be a better approximation.

The t_d/T_1 ratio for the three targets are:

Core Barrel	$t_d/T_1 = 4.4 \times 10^{-5}$
Thermal Shield Flexure	$t_d/T_1 = 0.0117$
Instrument Tube	$t_d/T_1 = 0.0024$

From these values of t_d/T_1, and recognizing that the t_d predicted may be low by a factor of 2 to 3 times, general observation in regard to effective target mass can be made:

1) Core barrel — The effective mass of the core barrel during impact is clearly that of a higher mode associated with local deflection of the core barrel shell in the region near the point of impact;

2) Thermal shield flexure— The effective mass is also that of a higher mode associated with local deflection.

3) Instrument tube — The value of t_d/T_1 indicates that the minimum mass should be used for the impact. However,

as shown on figure 3-4b, a substantial portion of the cantilever beam is above the point of impact on the beam. For movement to occur at the point of impact, the top portion must also move; thus the portion of the beam above the impact point will tend to act as a concentrated mass at the point of impact.

Although the determination of the effective mass is a complex problem which requires testing and refined analysis to define accurately, the best assumptions regarding the various targets are:

1) Core barrel -- M_e is the mass of the core barrel shell computed by the minimum mass criteria--for a missile cross section of 0.2" diameter the mass is 0.0174 $\frac{\text{lb sec}^2}{\text{in.}}$

2) Thermal shield flexure -- The flexure mass should be the M_e based on minimum mass criteria.

3) Instrument Penetration -- The instrument penetration M_e should be the mass above the impact point plus the portion of beam below the impact point for the mass coefficient from Table 3-4 for elastic conditions.

3.3.2.2 Coefficient of Restitution

The coefficient of restitution, e, is a measure of the energy loss during the collision of two bodies. The collision when e = 1 is referred to as a perfectly elastic collision, while when e = 0 the collision is classically referred to as a perfectly plastic collision. Collision with e between 0 and 1 are referred to as inelastic collision. Typically, the amount of permanent deformation in the bodies is used to illustrate the concept of the coefficient of restitution. The typical discussion on coefficient of restitution is misleading since it implies the energy dissipated during collision is only due to plastic deformation. In fact, energy during collision is dissipated by many mechanisms such as:

a) internal material damping;
b) internal vibrations of the bodies;
c) stress wave propagation from the point of impact;
d) friction at the contact surfaces; and
e) local and overall plastic deformations.

In many cases, a substantial energy loss can occur, with "e" approaching zero, without plastic deformation of the bodies during impact. An example is shown in figure 3-9 for a footing. In this case, a substantial portion of the input energy (by impact or vibration) is transmitted away from the point of contact by stress waves, which are losses during the energy transfer during impact, and thus do not participate in the overall deformation of the structure.

The actual coefficient of restitution is highly dependent on the size, shape, material properties and velocity of the bodies during collision. These characteristics are not only important because they affect plastic deformation of the bodies, but also they greatly affect the energy dissipated by other mechanisms.

Reliable values for "e" must be based on tests of similar missile and target geometries, or by extrapolation of test data. A conservative value of e = 0.8 is used in the analysis for determining damage to the target structures.

3.3.2.3 TARGET ENERGY ABSORPTION REQUIREMENTS

The table below summarizes the energy that must be absorbed by the three defined target structures based on the assumptions for M_e from Section 3.3.2.1 and a coeffcient of restitution (e) equal to 0.8. Section 3.3.3 discusses the consequent effects on the target structures.

Target Structure	E (in-lb)
Core Barrel	0.223
Instrument Tube (Bending Strike)	0.0887
Instrument Tube (Shear Strike)	(rigid target Assumed)
Thermal Shield Flexure	(rigid target assumed)

3.3.3 ENERGY ABSORPTION CAPABILITY OF TARGETS

After the energy that must be absorbed is known, the energy absorption capability of the structure is determined from the area under the resistance (force)-displacement curve. Figure 3-10 shows a typical curve. This area represents the strain energy absorption capability of the structure and must be equal to, or greater than, the energy of the impact discussed in Section 3.3.2. When the strain absorption capability is greater than the effective impact energy, the amount of permanent deflection in the structure can be estimated from the curve by assuming that unloading will occur along a line parallel to the original elastic portion of the curve. The intersection of the line with the deflection axis is an estimate of the permanent deflection in the structure due to impact.

The value R_m is the static collapse load and is that value of load that results in the formation of sufficient plastic hinges in the structure to create an unstable mechanism which would collapse without any additional load. The methods for computing the collapse load R_m are contained in many standard text books, and figures 3-11 and 3-12 provide the formulae for several common structures. The values in figure 3-11 and 3-12 are defined in terms of the plastic moment (M_u). The value of M_u is a function of the assumed stress-strain curve of the material and the geometry of the cross section of the beam or plate.

The most common assumption for the stress-strain relationship is that of elastic-perfectly plastic behavior. This assumption is consistent with that used in ASME subsections NB and NG for computing the collapse loads C_L and L_L, respectively. Therefore, the equivalent impact force to absorb the impact energy is comparable to the code limits for C_L and L_L. The cross section property, the plastic modulus, which is needed to compute M_u is contained in many common text books.[12]

The next parameter to be defined is the yield stress value for the material where perfect plastic behavior begins. The yield stress is assumed to be 1.5 S_m. The yield value is then increased by a conservative factor of 1.2 to account for the increase in yield stress due to the rapid strain rate during impact.

The increase in yield stress and ultimate stress, because of rapid strain rate, is well documented. In Ref. 7, tests were conducted with a range of strain rate of 10^{-6} to 10^3 per sec and for temperatures from about 25 to 600 °C. At room temperature, the increase in ultimate stress was 40 percent at the highest strain-rate, and the increase in yield stress was 170 percent. The normal rate of strain for tensile tests is about 2×10^{-3} per sec. The strain-rates, based on the impact velocity for the missiles considered herein, would be between 1×10^2 to 5×10^2. Thus the use of the common impact yield stress increase factor of 1.2 is considered very conservative for this evaluation.

0583E:1

It should be emphasized that the collapse load calculated using these assumptions is not the true collapse load of structures made from stainless steel. The "true" collapse load should be based on the ultimate strength and an elastic-strain hardening model for the material. These assumptions will increase the collapse load and energy absorption capability 1.5 to 2.0 times those calculated using the elastic-perfectly plastic assumption.

The preceeding discussion provides the procedure to calculate the strain energy absorption capability for structures that are not subject to other loads during the impact. In general, this is not the case, and the energy absorption capability of the structure must be reduced to reflect both sustained load and cyclic loads that exist concurrent with the impact. Figure 3-13a and b provide the energy reduction for a fixed-fixed beam for various potential concurrent load conditions for both the center impact and end impact loading.

Cases a and b on figures 3-13a and b are determined by calculating an equivalent load at the impact point (P') that results in an energy reduction equal to the indicated distributed or concentrated load. The equivalent load is given by:

$$\Delta P' = \int_0^b p(x)\, \phi(x)\, dx$$

Where:

Δ = the displacement at the point of impact

$p(x)$ = the concurrent load as a function of the length along the beam, and,

$\phi(x)$ = the elastic or plastic deformed shape as appropriate.

The value of P' varies as plastic hinges are formed during the impact, because the function $\phi(x)$ varies. In the calculations herein, the largest P' was used for the various elastic and hinge combinations that exist until the final collapse mechanism has been developed in the structure.

0583E:1

Concurrent loads such as load case c on figures 3-13a and b, do not in general affect the collapse load; however, they do affect the available energy up to the time that the collapse load mechanism is formed. Such loads increase or decrease the moment capacity at any beam location until a hinge is formed. The remaining moment capacity is:

$$M_R = M_u \pm M_i$$

Where:

M_R is the remaining moment capacity at a given location;
M_u is the plastic moment; and
M_i is the moment at a given location due to the concurrent load.

The remaining moment capacity at a location on the beam can change the applied load at which a hinge is formed and also can change the sequence that hinges are formed until the collapse load is reached. The reduction shown on figures 3-13a and b were determined by performing an analysis to determine the sequence of hinge formation for the indicated concurrent load.

The equivalent force P' for several concurrent cyclic loads that are independent, (caused by different sources of excitation, or are a result of different modes of vibration), should be combined by the Square-Root-of-the-Sum-of-the-Squares (SRSS) method to obtain the total P to be considered for the energy reduction. A cyclic load should be considered as a sustained load, if the cyclic period of the load, divided by 4, is greater than the anticipated time of the impact (time to reach the deformed shape required to absorb the effective impact energy in strain energy).

3.3.4 CORE BARREL ANALYSIS

Figure 3-2b shows the model used to evaluate the effect of the postulated impact on the core barrel. The loose part is assumed to impact the core barrel at the inlet nozzle at the inlet nozzle velocity. The minimum value of target effective mass and a coefficient of restitution (ϵ) equal to 0.8 were used in the analysis. The equivalent force (F_e) acting on the barrel, assuming elastic action of the barrel, is obtained by equating the energy (E) to be absorbed by the target (core barrel) to the strain energy of the barrel due to impact, or

$$E = (1/2)\, F_e \Delta = (1/2)\, K \Delta^2$$

where Δ = Deflection at point of impact

K = Equivalent spring constant at point of impact

The expressions for Δ and F_e are

$$\Delta = F_e / K$$

$$F_e = (2EK)^{1/2}$$

The value of K was determined based on the model shown in Figure 3-2b. the analysis performed counsidered both the local deflection of the shell and the deflection of the core barrel as a beam. The beam deflections are essentially negligible.

The K, ($K = F_e/\Delta$), is calculated from the deflection Δ given by Roark (5th edition, case 9b,/page 496):

$$\Delta = .0820\ B^5 F_e R^{3/4} L^{1/2} t^{-9/4} E_M^{\ -1}$$

where $B = [12(1-\mu^2)]^{1/8}$

R = mean radius of shell

L = length of shell

t = thickness of shell

E_M = elastic modulus

μ = poisson's ratio

The value of F_e is 652 lb.

The stresses in the barrel were also evaluated using the equations provided in Roark. The stress due to the impact, and the combined stresses for impact and normal operation are summarized in Table 3-5. The combined stresses are also compared to the allowables in Table 3-5.

As seen in Table 3-5, even using the most conservative assumption for energy absorption, the stresses are well within the allowable values.

Table 3-5 STRESS SUMMARY
CORE BARREL

SUMMARY OF APPLIED AND ALLOWABLE STRESS INTENSITIES FOR CORE BARREL AT POINT OF IMPACT

	P_m	$P_m + P_b$	$P_m + P_b + Q_m + Q_b$
Applied Stress Intensity	2,799	2,806	13,178
Allowable Stress Intensity	16,200 (S_m)	24,300 (1.5 S_m)	48,600 (3 S_m)
Factor of Safety	5.79	8.66	3.69

Stress Due To Impact of the parts are considered as secondary stresses.

3.3.5 INSTRUMENT TUBE ANALYSIS

As previously discussed, the penetrations are evaluated for two postulated hits. The first case is for maximum impact height above the reactor vessel. This is referred to as the "bending strike". The second case is for minimum height above the reactor vessel and is referred to as the "shear strike". The "bending strike" is discussed in section 3.3.5.1 and the "shear strike" is discussed in section 3.3.5.2.

3.3.5.1 Bending Strike

Figure 3-4b shows the model used to evaluate the effect of the impact on the tube of the penetration. The deflections of the tube at the point of impact includes both those due to bending and shear. In addition, the local rotational stiffness of the 5.5 inch thick reactor vessel was included. The overall bending stiffness of the reactor vessel was assumed rigid, and the rotational spring used in the analysis included the local stiffness of the vessel as an elastic half space. The rotational stiffness of a rigid circular disk on an elastic half space is (ref 20):

$$K_\theta = \frac{8Gr^3}{3(1-\mu)}$$

where: r is the radius of the tube which is equal to 0.75";
μ is poissions ratio; and the shear modulus
$G = E/2(1 + \mu)$

The resistance-displacement curve for the instrument tube is shown on figure 3-14. No other loads act on the tube concurrent with the impact. Thus the total area under the resistance-displacement curve is available to absorb the energy of impact. As previously discussed in section 3.3.2.1, the value which is appropriate for the target Mass (M_e) of the instrument tube is that which includes the weight of tube above the impact point, and the effective static deflected shape mass for the cantilever beam below the impact point. It is expected that a value for the coefficient of restitution of between 0 and 0.5

will exist for the actual missiles (part fragments) potentially involved in the impact. The actual part fragments are irregularly shaped and substantial local plastic deformation at the contact surfaces can be expected. However, there is little material in the literature that could be used to evaluate the actual value for "e". Thus, for the current evaluation, the conservative value of 0.8 is used.

Figure 3-14 shows the load and deflection that would occur to absorb the required strain energy for the e = 0.8 assumption. As seen on the figure, the energy would be absorbed without exceeding the conservatively defined collapse load of 1.2 L_L. In addition, the stresses predicted by elastic analysis as shown on the figure, are less than the value of (1.2) times 3 S_m. The impact force is a self limiting load condition, analogous to thermal loads, where the deflection of the structure, as shown on figure 3-14, is limited by the energy that it must absorb. Thus, secondary stress limits are applicable for the impact load condition.

Since the load is below the effective yield point of the tube, the permanent deflections are very small and neglected. The effective yield is defined as the load and corresponding deflection when the first plastic hinge is formed. This definition is, in general, more conservative than that normally used. The normal assumption is that the effective yield is the deflection based on the elastic load deflection curve at the collapse load. (e.g. the intersection of the horizontal collapse load line and the elastic load deflection line).

3.3.5.2 Shear Strike

Figure 3-4b shows the model used for the assumed missile impact at the junction of the penetration tube and the vessel. Preliminary calculations indicated that the tube is essentially rigid for this assumed impact condition. Thus, the bending strike model are not appropriate for the shear impact evaluation.

An alternative method was used to conservatively predict the load due to the shear strike . The tube was considered as a perfectly rigid body and the missile was assumed to remain perfectly elastic during the impact. As discussed in section 3.3.2.1, the constant contact pressure during impact is then given by:

$$P = \alpha C V_o;$$

and the contact time is given by:

$$t_d = 2L/C; \text{ where}$$

The terms are as defined in section 3.3.2.1. Since td/t is small, as seen in section 3.3.2.1, the maximum dynamic loading factor for a rectangular force-time history is 0.3. The maximum force for shear strike is

$$F_s = 0.3\ AP$$

where

A is the contact area during the strike

The contact area for the potential strike is conservatively assumed to be equal to a width of .25 inches times a length equal to one half of the tube outside diameter. The contact area is then .1875 square inches. For an impact velocity of 35.61 ft/sec, the force is then

$$F_s = 0.3 \times 0.1875 \times 58.3$$
$$= 3.3 \text{ kips}$$

The average primary pure shear in the tube is then 2.27 KSI. This stress is small in comparison with ASME Subsection NB allowable for pure shear which is 0.6 Sm or 14 KSI.

3.3.6 THERMAL SHIELD FLEXURE ANALYSIS

The thermal shield flexure is analyzed for two postulated impacts. The analysis is presented in sections 3.3.6.1 and 3.3.6.2.

3.3.6.1 Impact at Center of Thermal Shield Flexure

The load due to impact for this case is calculated assuming the minimum effective mass of the target and a coefficient of restitution of 0.8. The load-deflection relationship for a center load on the flexure is shown in Figure 3-17, corrected for the effect of simultaneous operating loads. For a minimum target effective mass of 7.21×10^{-5} $Lb\text{-}sec^2/in$ the energy that must be absorbed by the flexure is calculated to be 1.730 inch pounds. From Figure 3-17 it is seen that the spring rate in the elastic range of the load-deflection curve is [ ]a,b The load at which the required energy is absorbed is [ ]a,b pounds. From Figure 3-17 it is seen that for the center strike the flexure is able to withstand this load elastically. Therefore, no permanent set will occur and the flexure will remain structurally adequate.

3.3.6.2 Impact Near Flexure Support

For this case the minimum target mass is again assumed along with a coefficient of restitution of 0.8. Figure 3-18 is the load-displacement curve for a strike 1.708 inches from the flexure support, corrected for simultaneous operating loads. From this figure it is seen that the required energy is absorbed at a load of 2527 lb. Under this load, a single plastic hinge is formed in the flexure. The resultant permanent set in the flexure for a single impact is 0.00062 inches, which will not affect the structural integrity of the thermal shield flexure. Subsequent impacts are not expected to increase this permanent set due to material strain hardening.

3.4 SUMMARY IMPACT EFFECTS

The following is a summary of the work completed to evaluate the potential damage that may result due to the effects of loose parts impacting against the core barrel, thermal shield flexures and bottom mounted instrumentation tubes. The current work is based on a conservative estimate of the damage that could result from the impacting of the largest loose part found in the vessel. The analysis considers both the potential for perforation by the parts, as well as overall structure damage. The evaluations used the ASME code properties of the various target materials at 650^{0}F. The missiles were assumed to be traveling at the velocity of the coolant at the target to estimate the missile kinetic energy.

The potential for perforation was estimated by assuming failure by local shear mechanism that results in punching out a plug of the targest material. The energy required to punch out a plug of material and kinetic energy of missiles were than calculated. The smallest margin of safety calculated is 182.

The above method were also used to conservatively estimate the potential for penetration or denting. The predicted dent is quite small. The maximum depth of dent is 0.001".

In order to evaluate the overall response of the targets (structures) for missile impact, the evaluation for potential damage was performed using the conservative assumption of hard impact.

Conservation of momentum and energy are used to determine the portion of the kinetic energy of the missile that is transmitted to the structure to be absorbed as strain energy.

The strain absorption capability of the structures was determined both by elastic analysis and by plastic collapse load analysis. (The core barrel was only analyzed by elastic analysis and shown adequate)

In the collapse load analysis, the assumption for the stress-strain relationship is that of elastic-perfectly plastic behavior. This assumption is consistent with that used in ASME Sec. III, subsections NB and NG for computing the collapse loads C_L and L_L, respectively. The yield stress value for the material where perfect plastic behavior begins is assumed to be 1.5 S_m. The yield is then increased by a conservative factor of 1.2 to account for the increase in yield stress due to the rapid strain rate during impact. The energy absorption capability of the structure was reduced to reflect both sustained load and cyclic loads that exist concurrent with the impact.

A summary for the three defined targets is:

1. CORE BARREL ANALYSIS

The missile energy is assumed to be absorbed by the core barrel in elastic strain energy. The value used in the analysis was for the conservative assumption of minimum target mass and a coefficient of restitution (e) equal to 0.8.

The stresses were calculated for both the overall response of the core barrel, and the local shell stresses at the point of impact. The impact stresses when combined with the normal operating stresses are within allowable values.

2. INSTRUMENT TUBE ANALYSIS

The penetrations are evaluated for two postulated hits. The first case is for maximum impact height above the reactor vessel. This is referred to as the "bending strike". The second case is for minimum height above the reactor vessel, and is referred to as the "shear strike".

The instrument tube is able to withstand either of the postulated impact strikes.

3. THERMAL SHIELD FLEXURE ANALYSIS

The thermal shield flexure was analyzed for impacting loose parts at two postulated locations - at the center of the flexure and near the flexure support. The flexure was shown to be structurally adequate for both of the postulated impact strikes.

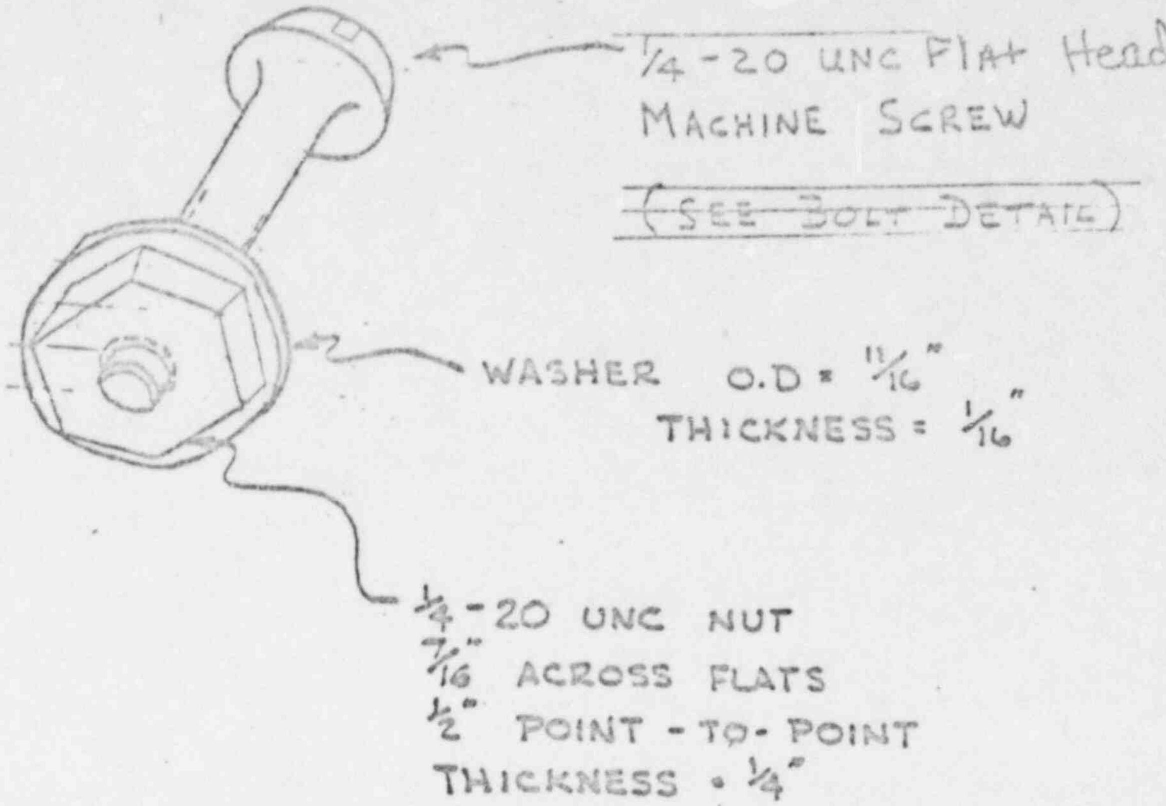

ALL PARTS STAINLESS STEEL
OVERALL LENGTH = 3/4 INCH
WEIGHT OF ASSEMBLY = 0.3 OUNCE

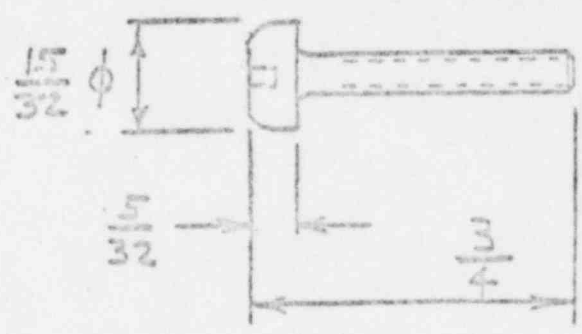

BOLT DETAIL

FIGURE 3-1a LOOSE BOLT ASSEMBLY

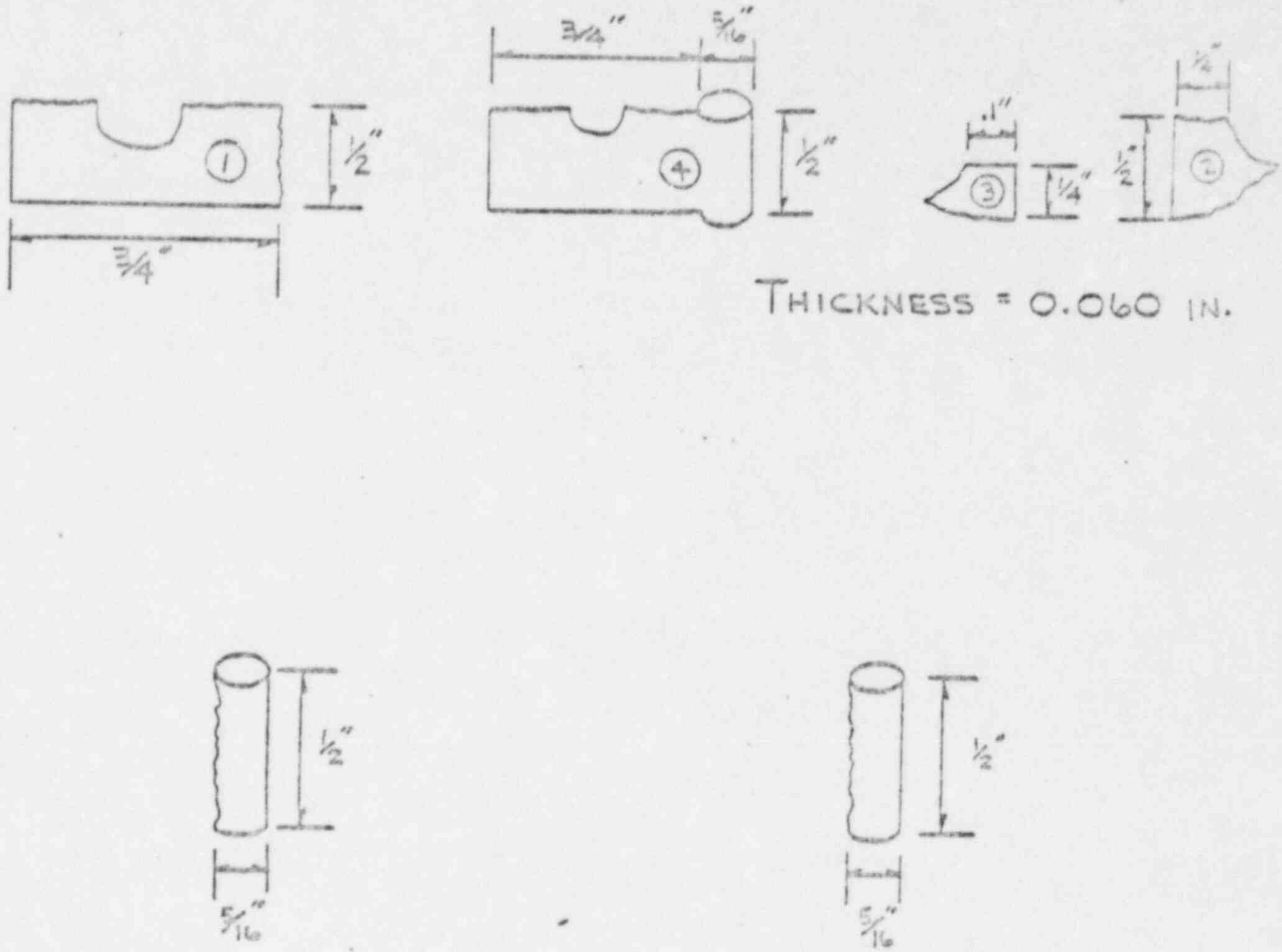

FIGURE 3-1b HINGE FRAGMENTS

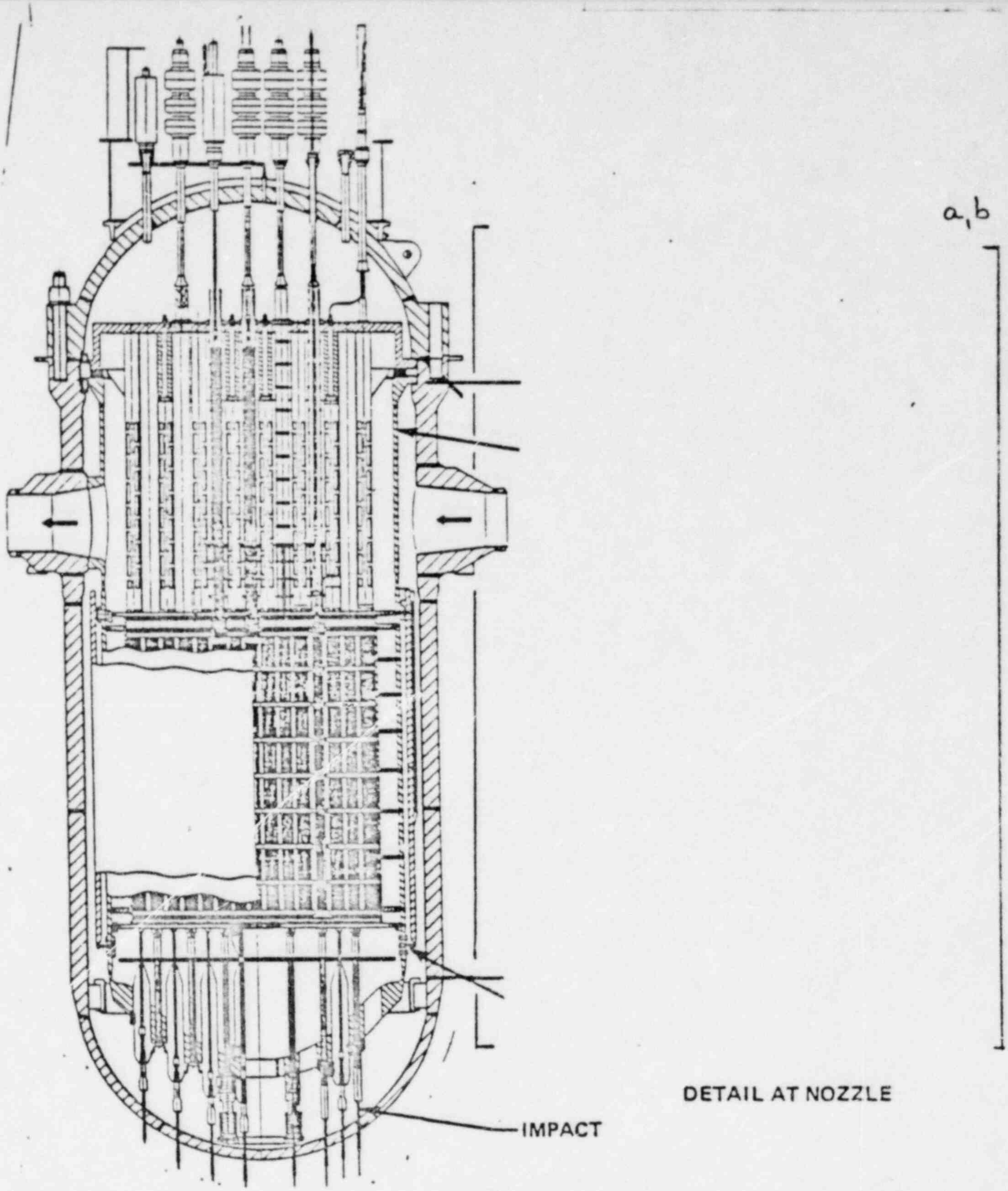

REACTOR VESSEL GENERAL ASSEMBLY

Figure 3-2a. Actual Core Barrel Configuration

a,b

Figure 3-2b. Idealized Core Barrel (Local Model)

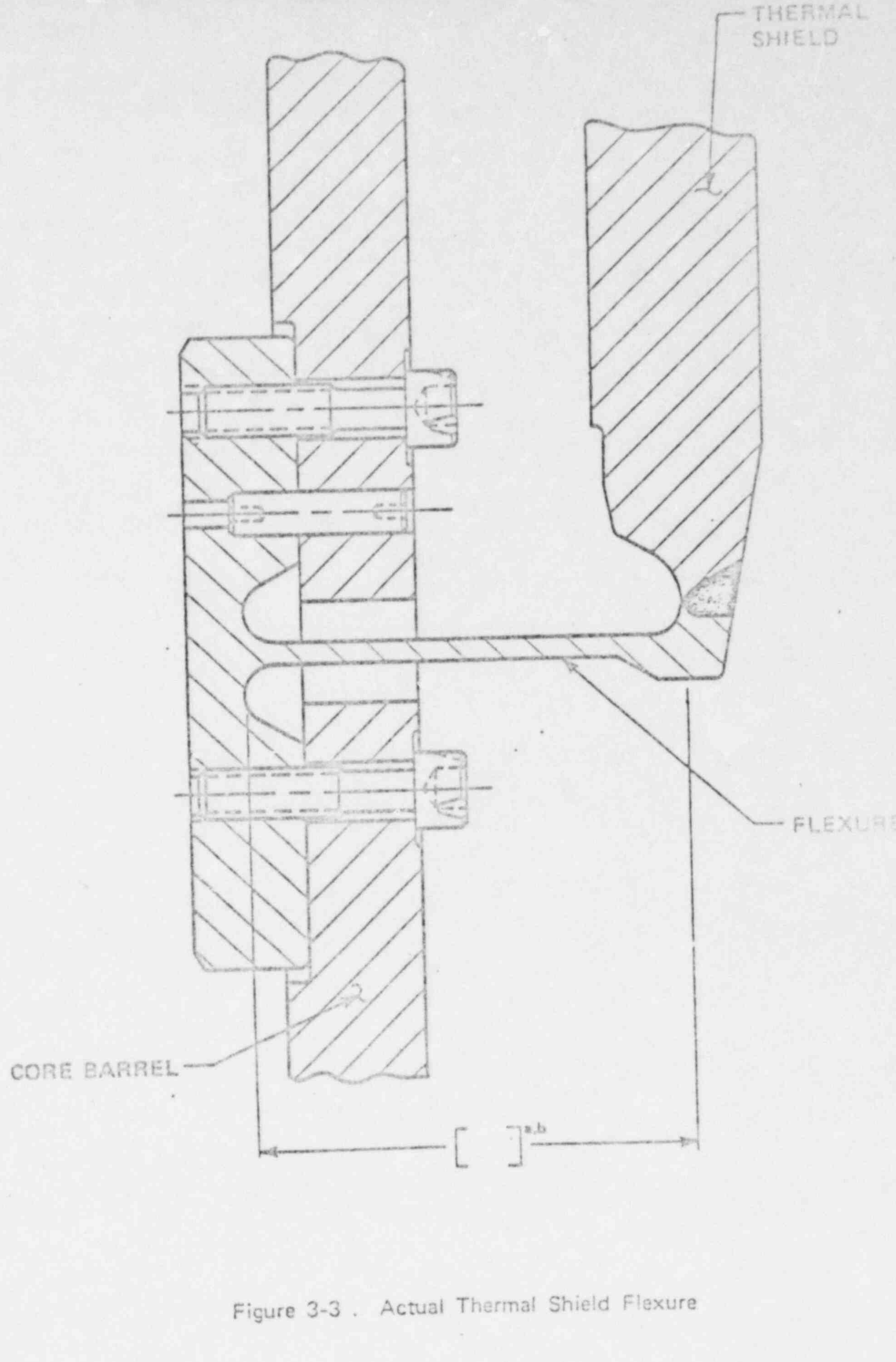

Figure 3-3 . Actual Thermal Shield Flexure

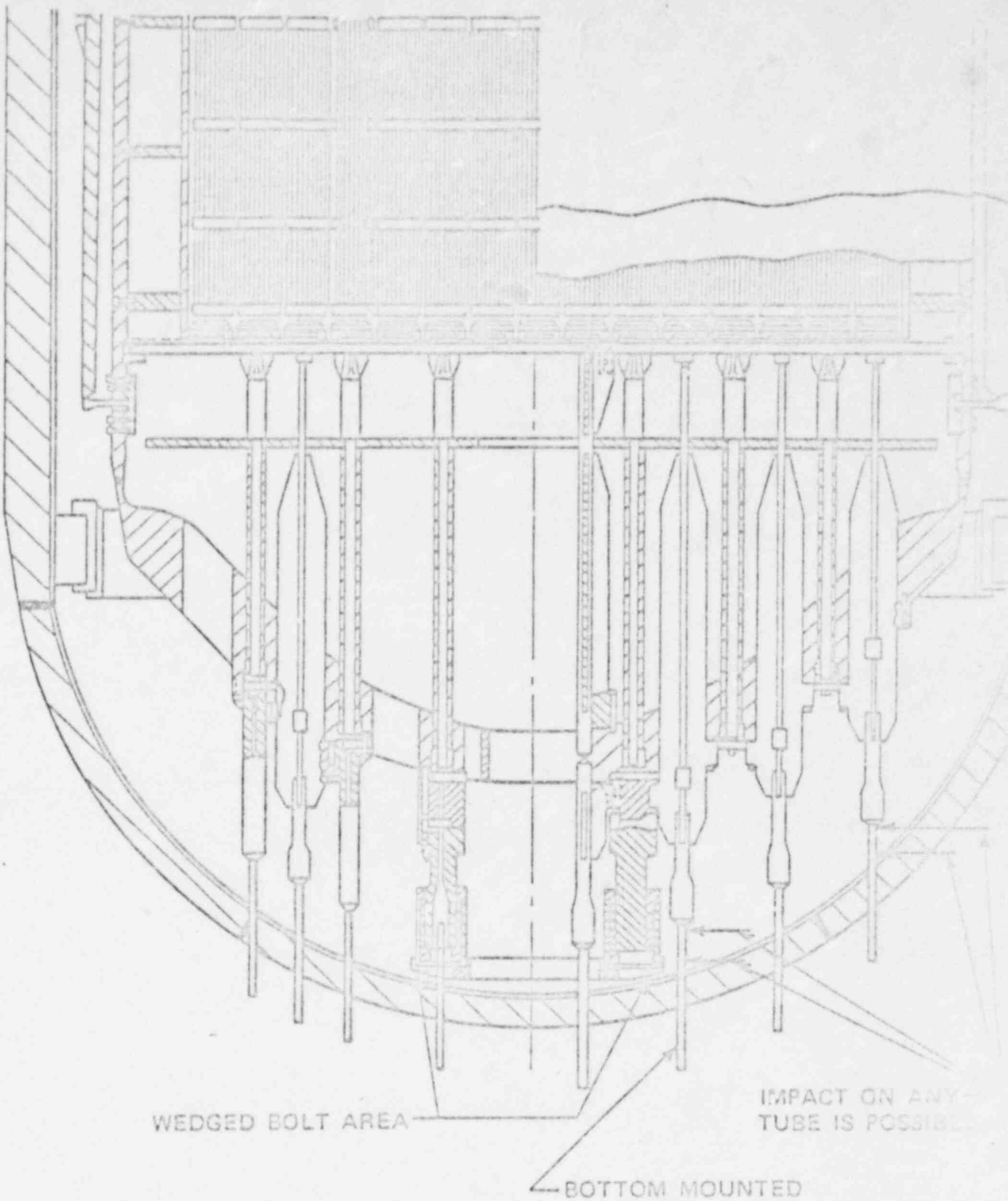

Figure 3-4a. Actual BMI Penetration Configuration

[ ][a,b]

IDEALIZED BMI PENETRATION (BENDING STRIKE)

[ ][a,b]

IDEALIZED BMI PENETRATION (SHEAR STRIKE)

Figure 3-4b. Idealized BMI Penetration Configuration

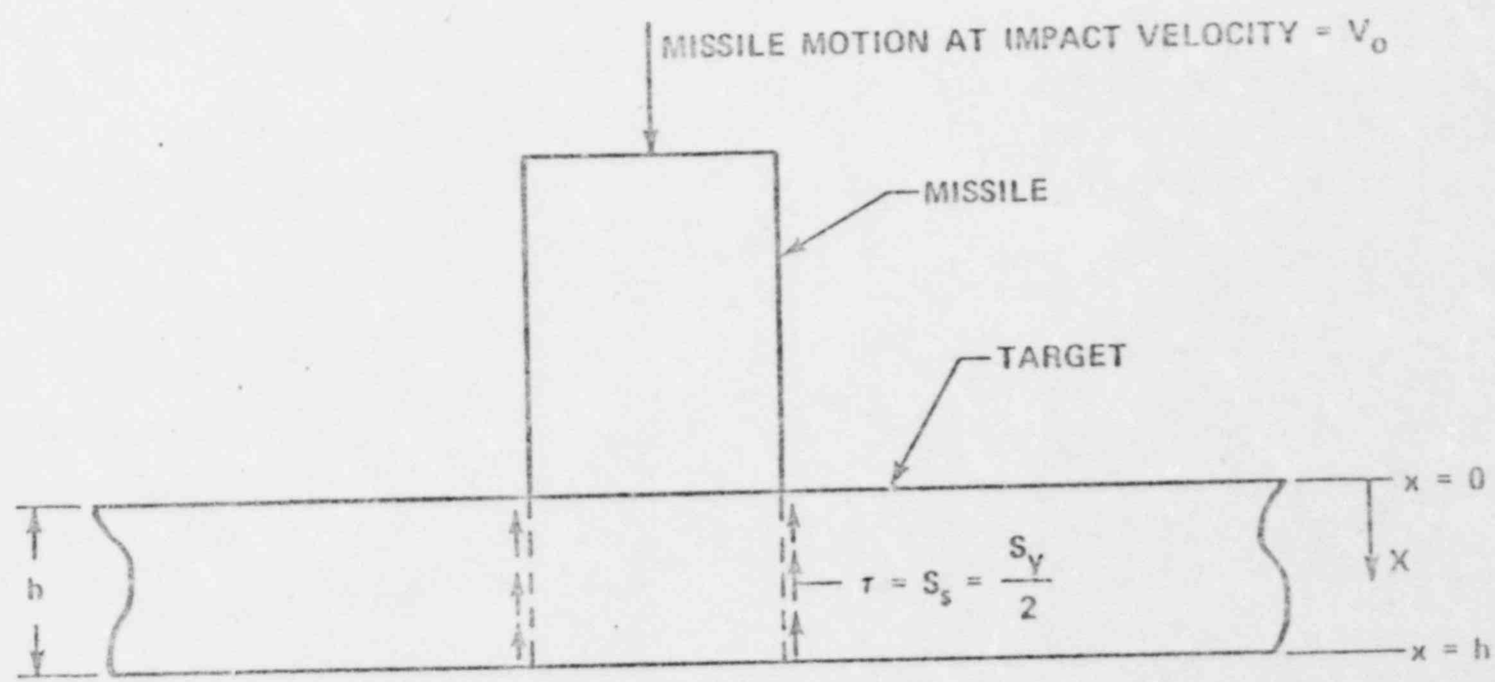

PUNCHING SHEAR MODEL

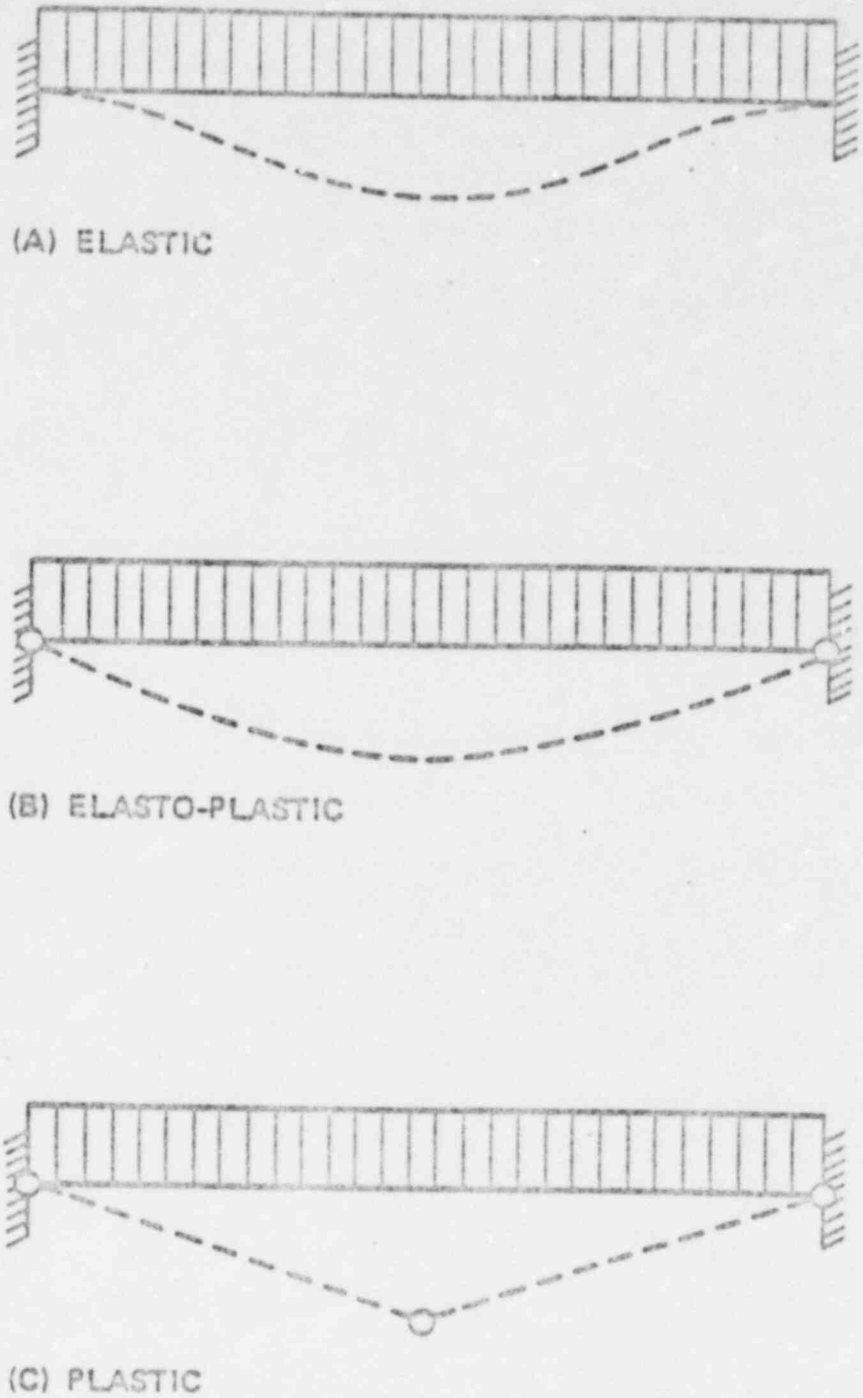

Figure 3- 6 Assumed Static Deformed Shapes for Determination of Effective Mass

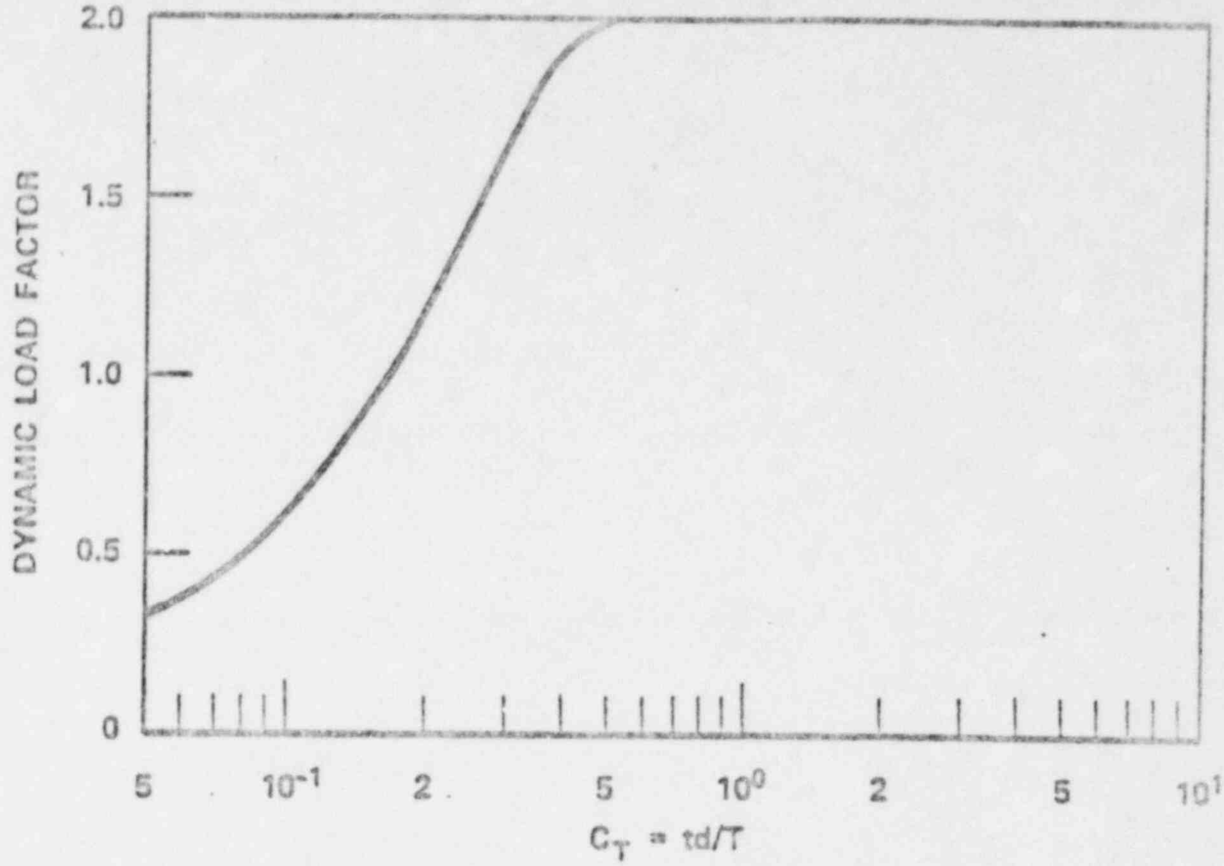

Figure 3-7. Dynamic Load Factor for Linear Elastic System Rectangular Impulse Load (From Ref 12)

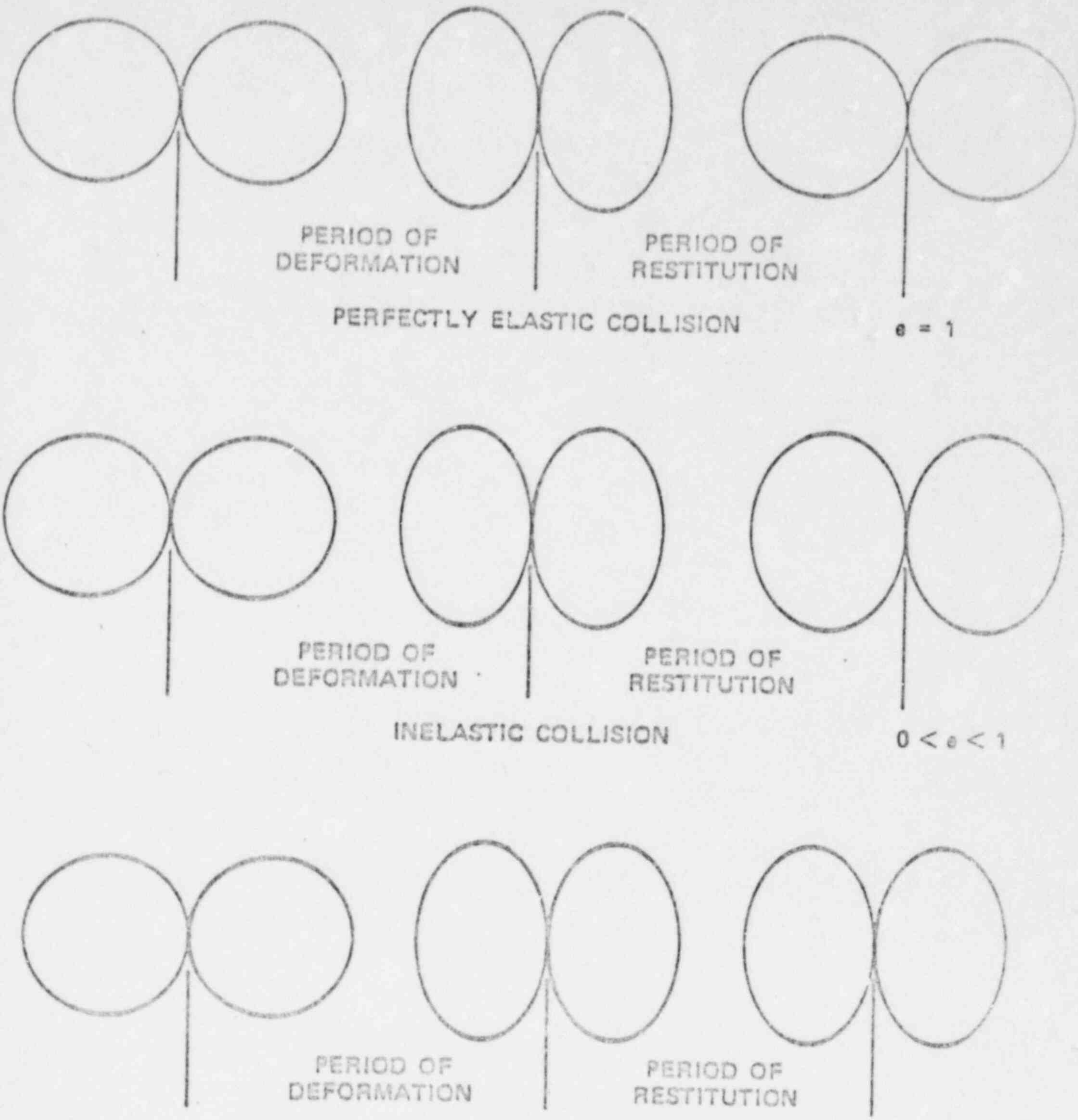

Figure 3-8. Deformation During Collision

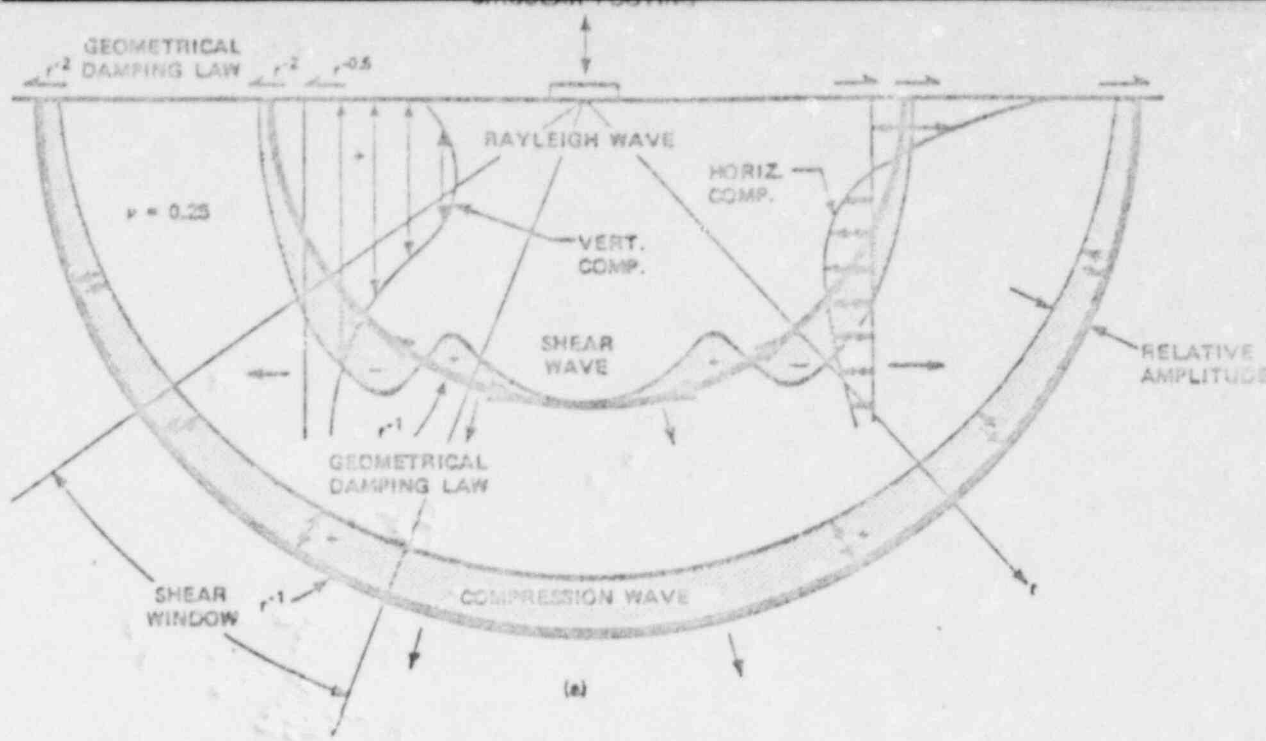

(a)

(b)

WAVE TYPE	PER CENT OF TOTAL ENERGY
RAYLEIGH	67
SHEAR	26
COMPRESSION	7

THE BASIC FEATURES OF THIS WAVE FIELD AT A RELATIVELY LARGE DISTANCE* FROM THE SOURCE ARE SHOWN IN FIG. 3-12a. THE DISTANCE FROM THE SOURCE OF WAVES TO EACH WAVE FRONT IN FIG. 3-12a IS DRAWN IN PROPORTION TO THE VELOCITY OF EACH WAVE FOR A MEDIUM WITH ν = 1/4. THE BODY WAVES PROPAGATE RADIALLY OUTWARD FROM THE SOURCE ALONG A HEMISPHERICAL WAVE FRONT (HEAVY DARK LINES IN FIG. 3-12a) AND THE RAYLEIGH WAVE PROPAGATES RADIALLY OUTWARD ALONG A CYLINDRICAL WAVE FRONT.

*ACCORDING TO LYSMER (REF. 14), A DISTANCE OF 2.5 WAVE LENGTHS FROM THE SOURCE IS A LARGE DISTANCE.

Figure 3-9 . Distribution of Displacement Waves From a Circular Footing on a Homogeneous, Isotropic, Elastic Half-Space (From Ref. 13)

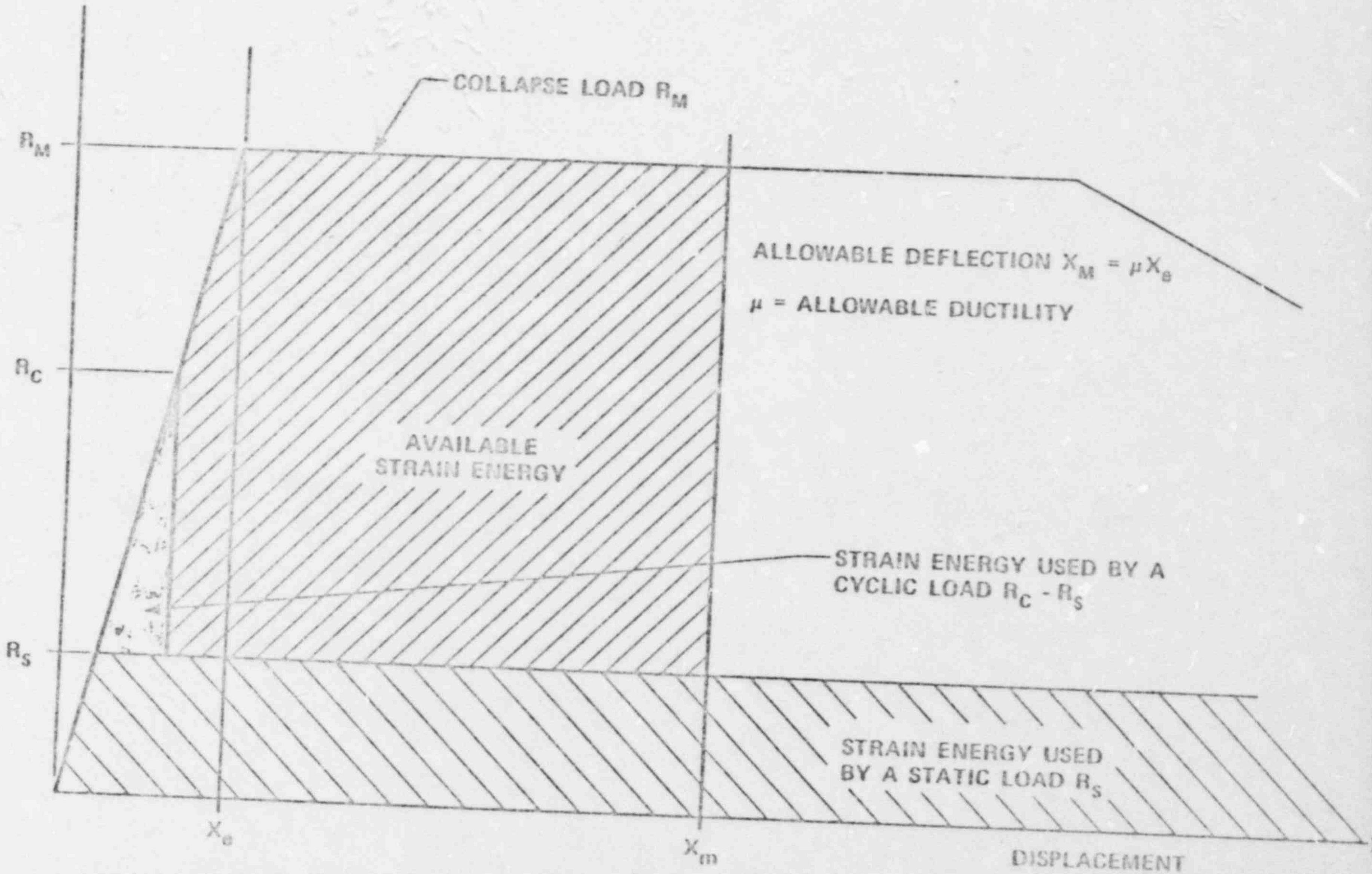

Figure 3.10. Resistance – Displacement Curve Showing Available Strain Energy

DESCRIPTION	RESISTANCE	STIFFNESS
(1) CANTILEVER 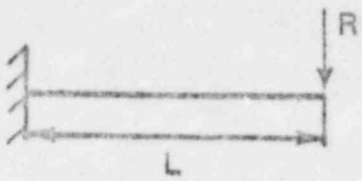	$R_M = \frac{M_u}{L}$	$K = \frac{3EI}{L^3}$
(2) SIMPLY SUPPORTED 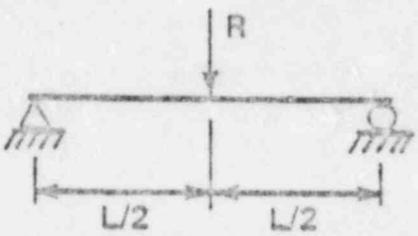	$R_M = \frac{4M_u}{L}$	$K = \frac{48EI}{L^3}$
(3) FIXED SUPPORTS 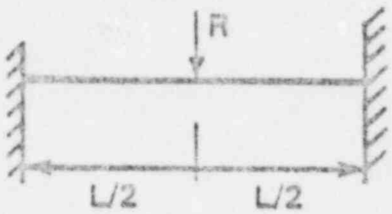	$R_M = \frac{4(M_u^+ + M_u^-)}{L}$	$K = \frac{192EI}{L^3}$
(4) MULTI-SPAN 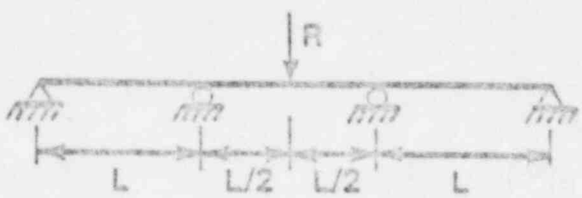	$R_M = \frac{4(M_u^+ + M_u^-)}{L}$	$K = \frac{92EI}{L^3}$

WHERE M_u^+ = ULTIMATE POSITIVE MOMENT CAPACITY

M_u^- = ULTIMATE NEGATIVE MOMENT CAPACITY

I = MOMENT OF INERTIA (in.^{4})

Figure 3-11. Stiffness and Resistance Values for Beams

DESCRIPTION	RESISTANCE	STIFFNESS

(1) SIMPLY SUPPORTED ON ALL 4 SIDES WITH LOAD AT CENTER

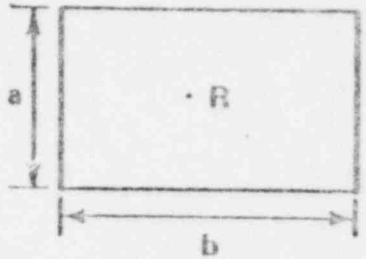

$$R_M = 2\pi M_u$$

$$K = \frac{12EI}{\alpha a^2 (1 - \nu^2)}$$

b/a	1.0	1.1	1.2	1.4	1.6	1.8	2.0	3.0	∞
α	.1390	.1518	.1624	.1781	.1884	.1944	.1981	.2029	.2031

ν = POISSON'S RATIO

t = THICKNESS (in.)

E = MODULUS OF ELASTICITY (lb/in.^{2})

I = MOMENT OF INERTIA PER UNIT WIDTH (in.^{4}/in.)

M_u^+ = ULTIMATE POSITIVE MOMENT CAPACITY (in./lb/in.)

M_u^- = ULTIMATE NEGATIVE MOMENT CAPACITY (in./lb/in.)

(2) FIXED SUPPORTS ON ALL 4 SIDES WITH LOAD AT CENTER

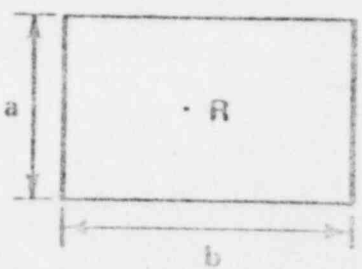

$$R_M = 2\pi (M_u^+ + M_u^-)$$

$$K = \frac{12EI}{\alpha a^2 (1 - \nu^2)}$$

b/a	1.0	1.2	1.4	1.6	1.8	2.0	∞
α	.0671	.0776	.0830	.0854	.0864	.0866	.0871

Figure 3-12 Stiffness and Resisting Values for Plates and Slabs Under Concentrated Loads

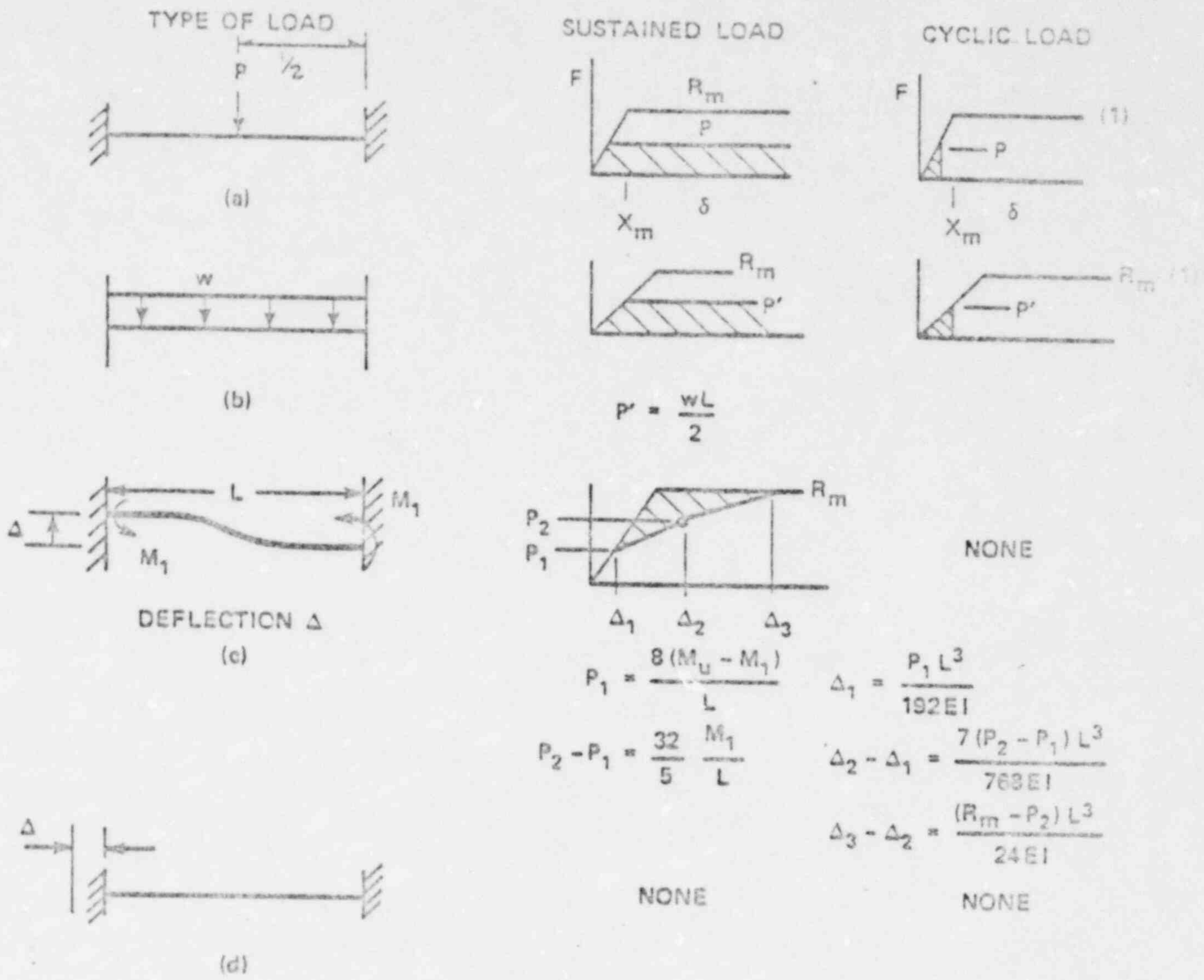

$$P' = \frac{wL}{2}$$

$$P_1 = \frac{8(M_u - M_1)}{L} \qquad \Delta_1 = \frac{P_1 L^3}{192EI}$$

$$P_2 - P_1 = \frac{32}{5}\,\frac{M_1}{L} \qquad \Delta_2 - \Delta_1 = \frac{7(P_2 - P_1)L^3}{768EI}$$

$$\Delta_3 - \Delta_2 = \frac{(R_m - P_2)L^3}{24EI}$$

LOADS THAT DO NOT CAUSE BENDING IN THE PLANE OF THE BEAM DO NOT EFFECT THE ENERGY ABSORPTION; BUT SHOULD BE CONSIDERED WHEN TOTAL STRAINS ARE EVALUATED.

(hatched box) = LOST ENERGY

(1) THE EFFECTIVE FORCE P FOR SEPARATE CYCLIC EXCITATION CONDITIONS SHOULD BE COMBINED BY THE SRSS METHOD.

IMPACT AT CENTER
FIXED – FIXED BEAM

Figure 3-13a. Energy Reduction for Concurrent Loads

TYPE OF LOAD | SUSTAINED LOAD | CYCLIC LOAD

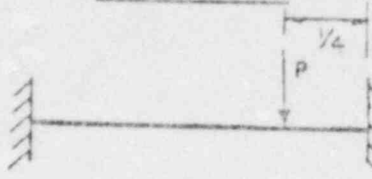

(a)

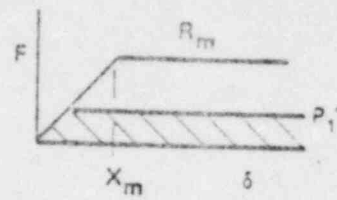

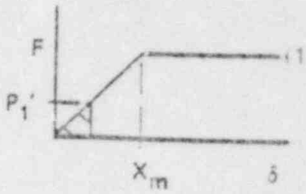

$P_1' = 1.540\,P$

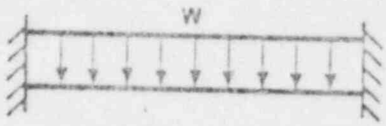

(b)

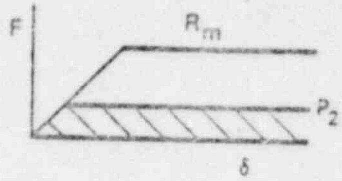

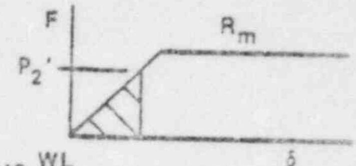

$P_2' = 1.540\,\frac{WL}{2}$

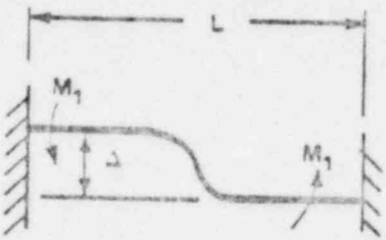

DEFLECTION Δ

$M_1 = \frac{6EI\Delta}{L^2}$

(c)

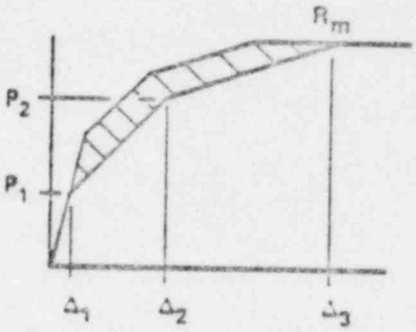

NONE

$P_1 = \frac{7.111}{L}(M_p - M_1)$

$P_2 = \frac{.790}{L}(13M_p - M_1)$

$R_m = \frac{10.667}{L}M_p$

$\Delta_1 = \frac{L^2}{64EI}(M_p - M_1)$

$\Delta_2 = \frac{L^2}{EI}(0.0382\,M_p + 0.0295\,M$

$\Delta_3 = \frac{L^2}{EI}(0.0937\,M_p + 0.1406\,M$

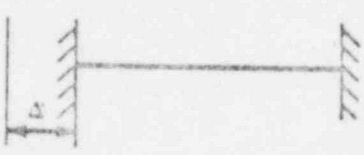

(d)

LOADS THAT DO NOT CAUSE BENDING IN THE PLANE OF THE BEAM DO NOT AFFECT THE ENERGY ABSORPTION, BUT SHOULD BE CONSIDERED WHEN TOTAL STRAINS ARE EVALUATED.

 = LOST ENERGY

IMPACT AT POINT L/4 FROM SUPPORT
FIXED-FIXED BEAM

Figure 3-13b. Energy Reduction for Concurrent Loads

a,b

Figure 3-14 Resistance – Displacement Function Instrument Penetrations

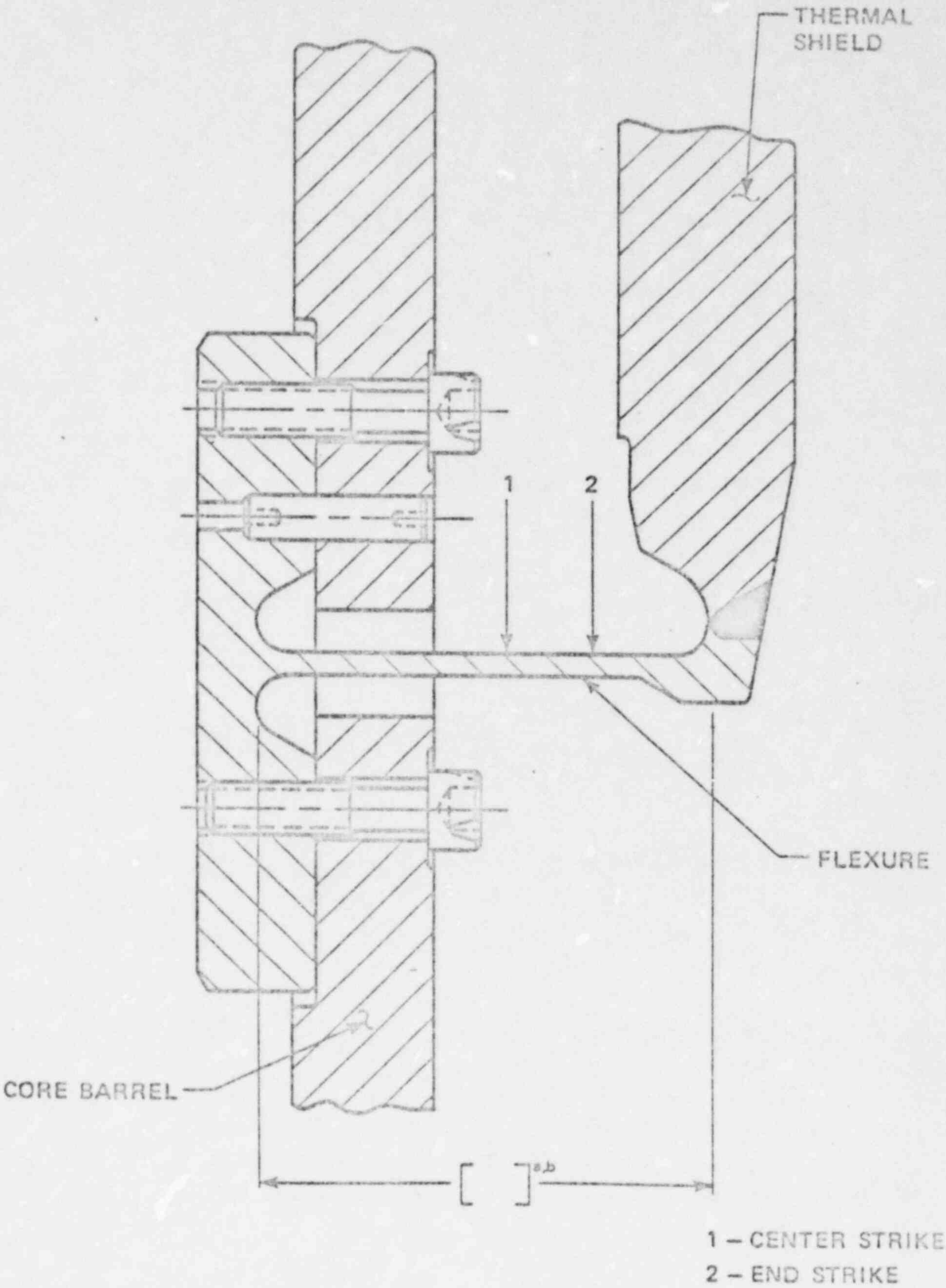

Figure 3-15 Actual Thermal Shield Flexure

[a,b]

Figure 3-16. Flexure Normal Loads (Concurrent Loads)

a,b

Figure 3-17. Resistance – Displacement Function Thermal Shield Flexures

a,b

Figure 3-18 Resistance – Displacement Function for Thermal Shield Flexures

4.0 REFERENCES

1. Singleton, N. R., Davidson, A. C., and Hluhan, R. A., "Phase I Analytical Assessment for Effect of Loose Parts Indian Point Plant Unit No. 2", WCAP-9934, 1981. (Westinghouse Proprietary).

2. Roark, R. J., and Young, W. C., "Formulas for Stress and Strain" McGraw-Hill, 5th Edition 1975.

3. "Reactor Coolant System Operating Limitations", Zion Plant, Unit No. 1, Telecopy Communication, May 4, 1982.

4. "WECAN - Westinghouse Electrical Computer Analysis User's Manual", Westinghouse Electrical Co.

5. Davidson, A. C., "Calculation Brief on IPP Unit No. 2, Section 2.0 Phase I Report", Unpublished report, 1981.

6. Richart, F. E. etal, "Vibrations of Soil and Foundations", Prentice-Hall, 1970.

7. Manjoine, M. J., "Influence of Rate of Strain and Temperature on Yield Stresses of Mild Steel", Trans. Amer. Soc. Mech. Engrs. J. App. Mech. Pages 211-218, 1944.

8. Williamson, R. A. and Ralvy, N. R., "Impact effects of Fragments Striking Structural Elements", Holmes and Nauer, 1973.

9. Linderman, R. B., et al, "Design of Structures for Missile Impact", BC-TOP-9-A, (Rev. 2), Bechtel Power Company 1974.

10. ANS-58.1 (ANSI-N177), Draft, "Plant Design Against Missiles", American Nuclear Society, August 1978.

11. Biggs, J. M., "Introduction to Structural Dynamics", McGraw-Hill, New York, 1964.

12. "Manual of Steel Construction", 7th Edition, American Institute of Steel Construction", 1973.